

This discussion paper is/has been under review for the journal Geoscientific Instrumentation, Methods and Data Systems (GI). Please refer to the corresponding final paper in GI if available.

CLUSTER STAFF search coils magnetometer calibration – comparisons with FGM

P. Robert¹, N. Cornilleau-Wehrlin^{1,2}, R. Piberne¹, Y. de Conchy², C. Lacombe², V. Bouzid¹, B. Grison³, D. Alison¹, and P. Canu¹

¹Laboratoire de Physique des Plasmas, CNRS, Palaiseau, France

²Observatoire de Paris, CNRS, Meudon, France

³Institute of Atmospheric Physics, Praha, Czech Republic

Received: 31 May 2013 – Accepted: 7 October 2013 – Published: 12 December 2013

Correspondence to: P. Robert (patrick.robert@lpp.polytechnique.fr)

Published by Copernicus Publications on behalf of the European Geosciences Union.

CLUSTER STAFF
search coils
magnetometer
calibration

P. Robert et al.

Title Page

Abstract

Introduction

Conclusions

References

Tables

Figures

⏪

⏩

◀

▶

Back

Close

Full Screen / Esc

Printer-friendly Version

Interactive Discussion

Abstract

The main part of Cluster Spatio Temporal Analysis of Field Fluctuations (STAFF) experiment consists of triaxial search coils allowing the measurements of the three magnetic components of the waves from 0.1 Hz up to 4 kHz. Two sets of data are produced, one by a module to filter and transmit the corresponding waveform up to either 10 or 180 Hz (STAFF-SC) and the second by an onboard Spectrum Analyser (STAFF-SA) to compute the elements of the spectral matrix for five components of the waves, $3 \times B$ and $2 \times E$ (from EFW experiment) in the frequency range 8 Hz to 4 kHz.

In order to understand the way the output signal of the search coils are calibrated, the transfer functions of the different parts of the instrument are described as well as the way to transform telemetry data into physical units, across various coordinate systems from the spinning sensors to a fixed and known frame. The instrument sensitivity is discussed. Cross-calibration inside STAFF (SC and SA) is presented. Results of cross-calibration between the STAFF search coils and the Cluster Flux Gate Magnetometer (FGM) data are discussed. It is shown that these cross-calibrations lead to an agreement between both data sets at low frequency within a 2% error. By means of statistics done over 10 yr, it is shown that the functionalities and characteristics of both instruments have not changed during this period.

1 Introduction

Data calibration of spectra and waveforms issued from a search coil magnetometer is not a new problem. Among previous space physics missions using search coils magnetometers, let's mention GEOS-1 and GEOS-2 as the first ESA spacecraft dedicated to the study of waves and particles in the magnetosphere (Knott, 1975; Jones, 1977). The GEOS wave consortium (S300 experiment) comprised a tri-axis search-coil magnetometer build by the ancestry of the spatial team of the LPP. The technology used in CLUSTER/STAFF experiment has been deeply upgraded since this epoch,

GID

3, 679–751, 2013

CLUSTER STAFF search coils magnetometer calibration

P. Robert et al.

[Title Page](#)

[Abstract](#)

[Introduction](#)

[Conclusions](#)

[References](#)

[Tables](#)

[Figures](#)

[⏪](#)

[⏩](#)

[◀](#)

[▶](#)

[Back](#)

[Close](#)

[Full Screen / Esc](#)

[Printer-friendly Version](#)

[Interactive Discussion](#)



**CLUSTER STAFF
search coils
magnetometer
calibration**

P. Robert et al.

[Title Page](#)[Abstract](#)[Introduction](#)[Conclusions](#)[References](#)[Tables](#)[Figures](#)[⏪](#)[⏩](#)[◀](#)[▶](#)[Back](#)[Close](#)[Full Screen / Esc](#)[Printer-friendly Version](#)[Interactive Discussion](#)

but the principle remains the same: how to calibrate magnetic waveforms issued from a search-coil rotating across a high ambient DC field, knowing that the transfer function is varying with the frequency? This kind of problems has been solved at this epoch for time-frequency studies (Robert et al., 1978, 1979). Nevertheless, since the creation of the CLUSTER Active Archive (Perry, 2005), the need of having a continuous calibrated waveform became essential, and a dedicated method, detailed in this paper, was deployed.

To calibrate a set of search-coil data is one thing, to be sure that the calibration is right is another thing. It is true for calibration of any instrument, but particularly important for search coils calibration where the solution is not unique. In fact, it depends of calibrations parameters, themselves depending of the frequency band of the signal (see Sect. 6.4) Using the amplitude of the spin tone measured in the spin plane by the search coil, it is possible to compute the two DC field components in this plane, and so compare it with a fluxgate magnetometer instrument. This has been done at the GEOS epoch, where the agreement found was $\sim 4\%$ on the magnitude and $\sim 4^\circ$ on the direction (Robert, July 1979).

As the CLUSTER data are archived and will be used a long time after the life duration of the instrument and corresponding PI and engineers, it was about time to do this work now to get the best possible calibration and to do needed checks of cross calibration. So a special care has been devoted to the calibration and the cross-calibration of the magnetic wave measurements, before launch on ground, then onboard during the commissioning phase and all along the mission. A special effort to compare STAFF-SC data with the FGM on board flux gate magnetometer data (Balogh et al., 1997, 2001) has been undertaken since the beginning of the mission until now. This was encouraged by the Cluster Active Archive (CAA) activities and particularly the organisation of regular Cross-Calibration meetings.

The present paper, after a short reminder of STAFF experiment (Sect. 2), presents the instrument transfer functions determined on ground, followed by the in flight verification (Sect. 3). Then comparison of the sensitivity of the instrument both on ground and

CLUSTER STAFF search coils magnetometer calibration

P. Robert et al.

[Title Page](#)

[Abstract](#)

[Introduction](#)

[Conclusions](#)

[References](#)

[Tables](#)

[Figures](#)

[⏪](#)

[⏩](#)

[◀](#)

[▶](#)

[Back](#)

[Close](#)

[Full Screen / Esc](#)

[Printer-friendly Version](#)

[Interactive Discussion](#)

in space is discussed (Sect. 4). The transformation of the raw data, that are acquired in a spinning system (Cluster spacecraft are spin stabilised) into a fixed physically meaningful reference frame needs a series of successive coordinate transformations described in Sect. 5. Then the conversion of telemetry data into physical units, that is to say the calibration process itself, is presented for the wave form data (Sect. 6) and for the Spectrum Analyser data (Sect. 7). The continuity of spectral values as well as the similarity in the wave characterisation between the two STAFF experiments is presented in Sect. 8. Section 9 is devoted to the comparison between STAFF and FGM data and to discussion of the obtained results, followed by the conclusion.

2 Instrument description

STAFF is one of the five experiments of the Wave Experiment Consortium (WEC), see Pedersen et al., 1997. The optimisation of the analysis of the five components of the electromagnetic waves is among the objectives of the WEC. The STAFF experiment comprises a boom-mounted three-axis search coil magnetometer, a preamplifier and an electronics box that houses the two complementary data-analysis packages: a digital Spectrum Analyser, and an on-board waveform unit. The experiment is briefly described below, with some emphasis on elements of interest for the further wave characteristic determination and the comparison between the four spacecraft. For a detailed description of the experiment, see Cornilleau-Wehrin et al. (1997, 2003). The search coils are mounted at the extremity of a radial boom to avoid interferences from the spacecraft. Figure 1 gives a schematic of the position of the STAFF antennas with respect to the spacecraft body axis.

The frequency range of the search coils measurements is 0.1 Hz to 4 kHz. The signals go to the preamplifiers which incorporate an order 1 high pass filter at 0.3 Hz in order to diminish the spin signal. Then the three output signals enter the waveform unit where the analog wave form signal is sent to different Cluster experiments. First inside the waveform unit it is filtered and digitized before being sent to DWP, the

Digital Wave-Processing experiment (Woolliscroft et al., 1997), interface between wave experiments and the spacecraft. Second it is sent to the STAFF Spectrum Analyser (STAFF SA) and to other experiments (see the STAFF block diagram on Fig. 2). Those are the Electron Drift Instrument (EDI) (Paschmann et al., 1997), Wide-Band Plasma Wave (WBD) (Gurnett et al., 1997) and the Electric Field and Wave experiment (EFW) (Gustafsson et al., 1997). The internal memory of EFW permits, among different possibilities, to get small snapshots of the 5 components waveform up to 4 kHz.

The magnetic waveform unit comprises low-pass filters of the seventh order, characterized by 3 dB attenuation at either 10 or 180 Hz, selected by telecommand in accordance with the telemetry rate. The sampling rate is 25 and 450 Hz respectively. The output signals are digitised in a real 16 bit analogue-to-digital converter. The 96 dB dynamic range allowed by the 16 bit digitalisation permits to analyse simultaneously natural waves of a few $10^{-5} \text{ nT Hz}^{-1/2}$ and the large signal induced by the rotation of the spacecraft in the environmental DC field, up to some 2 000 nT at 0.25 Hz. With such a dynamic range we can get accurate measurements, even at the inversion of the DC magnetic field e.g. at the magnetopause crossing. The experiment had been designed for its initial orbit for which the perigee was at a radial distance from Earth centre of 4 Earth radii. During the prolongation of the Cluster mission, due to mechanical laws, perigee has decreased a lot and there are periods around perigee where the waveform does saturate. While the data are useless for those periods, this has not induced a degradation of the experiment capabilities. Owing to telemetry limitations, a reduction of the dynamic data range from 16 to 12 bits is performed inside DWP. The principle is to transmit the full 16-bit word at the beginning of each telemetry packet, and later the difference between the successive samples, coded on 12 bits in such a way that the dynamics of the experiment is preserved even at boundary crossings. Conservative back-up solutions can be selected by telecommand, being either a more crude compression, or no compression at all. The back-up compression is used during three hours around perigee where the spin signal can be above some 200 nT, and in

CLUSTER STAFF
search coils
magnetometer
calibration

P. Robert et al.

[Title Page](#)[Abstract](#)[Introduction](#)[Conclusions](#)[References](#)[Tables](#)[Figures](#)[⏪](#)[⏩](#)[◀](#)[▶](#)[Back](#)[Close](#)[Full Screen / Esc](#)[Printer-friendly Version](#)[Interactive Discussion](#)

high telemetry rate were the waveform is acquired up to 180 Hz. The three modes have been successfully tested during the commissioning phase.

At higher frequencies for which the telemetry does not permit to get the waveform, an onboard Spectrum Analyser is part of the STAFF experiment. In addition to the three search coils output signals, the Spectrum Analyser receives the signals from the four electric field probes of the EFW experiment. These are used to form a pair of orthogonal electric field dipole sensors. All five inputs ($2 \times E + 3 \times B$) are used to compute in real time the 5×5 Hermitian cross-spectral matrix at 27 frequencies distributed logarithmically in the frequency range 8 Hz to 4 kHz. The components in the spin plane are despun onboard. All channels are sampled simultaneously, and the integration time for each channel is the same as the overall instrument time resolution, which can be commanded to values between 125 ms and 4 s. The five auto-spectral power estimates are obtained with a dynamic range of approximately 100 dB and an average amplitude resolution of 0.38 dB. The ten cross-spectral power estimates are normalised to give the coherence. The precision of the phase depends upon the magnitude of the coherence: for a signal with magnitude in the highest bin, it is approximately 5° close to 0° , 180° , and $\pm 90^\circ$, increasing to about 10° midway between these angles.

STAFF waveform box also houses an onboard calibration unit that permits to detect a potential failure of a part of the experiment and recalculate the transfer function in case of any variation of the experiment response, which is crucial for the comparison between the four spacecraft. The calibration sequence, run once every orbit, consists in sending successively a white noise and fixed frequency sine waves (~ 7 and 100 Hz), the intensity of which is diminished, step by step. The calibration signals are sent at the input of the search coil through the feedback wiring (Fig. 7 of Cornileau-Wehrin et al., 1997).

GID

3, 679–751, 2013

CLUSTER STAFF search coils magnetometer calibration

P. Robert et al.

[Title Page](#)

[Abstract](#)

[Introduction](#)

[Conclusions](#)

[References](#)

[Tables](#)

[Figures](#)

[⏪](#)

[⏩](#)

[◀](#)

[▶](#)

[Back](#)

[Close](#)

[Full Screen / Esc](#)

[Printer-friendly Version](#)

[Interactive Discussion](#)



angle between the spacecraft spin axis and the Z antennas is of the order of 0.5° . As it has been decided to do not take into account this small misalignment, it has been also decided to neglect the very small non orthogonality of the sensors.

3.2 Corrections applied to the initial transfer functions

While measurements during commissioning phase showed that the sensitivity and transfer functions were as expected from ground measurements (see Fig. 2 of Cornilleau-Wehrin et al., 2003), it appeared during scientific operation that we observed a systematic underestimation of SC1 measurements of about 10 % at low frequency, in particular at the spacecraft spin period. Moreover, comparisons of STAFF waveform data with FGM data evidenced another 10 % underestimation. The reasons of those differences have been studied and explained, leading to a correction of the transfer functions. It is those corrected transfer functions that are given in Figs. 3 and 4. Let's explain the different issues. First we look at the 10 % difference between SC1 and the others. Going back to records of measurements in Chambon-la-Forêt, we found that the current loop axis we used for SC1 was not the same as for the other spacecraft, and this explained the differences between SC1 and others. Then looking very carefully at each of the three current loops, we found that their structures were no longer perfect plane circles. In addition, the big loops aimed at compensating the DC Earth magnetic field which was aligned with the current loop axis used for SC1 antennas but not used for the other spacecraft search coils, disturbed the magnetic field by means of an induced magnetic field opposite to the one produced by the current loop even at very low frequencies. All this has been verified by means of a reference search coil (that has been tested with different Helmholtz Coil facilities and compared with predicted measurements). From this a corrective transfer function has been established:

$$FT_CORR = 1.1 \times \frac{(1 + j \frac{f}{f_{ch}})}{(1 + j \frac{f}{f_{cb}})}$$

CLUSTER STAFF search coils magnetometer calibration

P. Robert et al.

[Title Page](#)

[Abstract](#)

[Introduction](#)

[Conclusions](#)

[References](#)

[Tables](#)

[Figures](#)

[⏪](#)

[⏩](#)

[◀](#)

[▶](#)

[Back](#)

[Close](#)

[Full Screen / Esc](#)

[Printer-friendly Version](#)

[Interactive Discussion](#)



with $f_{ch} = 85$ Hz and $f_{cb} = 102$ Hz.

The new transfer functions thus obtained have been applied to STAFF data and compared again with FGM data, as will be shown later on in this paper, giving satisfactory results. Then it was estimated that we had found the error sources, and that we could not go further. This comparison seems to show that the facility loops had already undergone the deformation at the time of Cluster STAFF search coils calibration, in 1999, observed some years after.

As the site magnetic quietness is not perfect, there remains some variations in the transfer function which were attributed to the environmental electric array, namely at 50 and 150 HZ. This lead to smooth the new transfer function, as can be seen on Fig. 5.

3.3 Similarity of the search coils, between the three components and between the four spacecraft

As the aim of the Cluster mission is to perform tri-dimensional measurements, implying to be able to combine the data of the different spacecraft for either deriving quantities as curl to get e.g. small scale currents or to apply the so-called K -filtering method (Pinçon and Lefeuvre, 1991) to disentangle possible different waves modes in turbulent like wave spectra, it was a requirement to produce four experiments as similar as possible (see e.g. Fig. 4 in Cornilleau-Wehrlin et al., 1997). An example is given in Fig. 6 below, where it can be seen that the relative difference in response in amplitude of the transfer function in the frequency range 0.1–180 Hz is less than 2%. The normalised differences $B_x - B_y$, $B_x - B_z$ and $B_y - B_z$ are over plotted in red, green and blue respectively. For other spacecraft and for 10 Hz filters output the normalised differences have the same order of magnitude. Note that the differences start to increase around 180 Hz, where the low pass filters start to be efficient.

CLUSTER STAFF search coils magnetometer calibration

P. Robert et al.

[Title Page](#)

[Abstract](#)

[Introduction](#)

[Conclusions](#)

[References](#)

[Tables](#)

[Figures](#)

[⏪](#)

[⏩](#)

[◀](#)

[▶](#)

[Back](#)

[Close](#)

[Full Screen / Esc](#)

[Printer-friendly Version](#)

[Interactive Discussion](#)



3.4 In flight calibration

As mentioned above (Sect. 2), in order to verify the health of the experiment in operation, the in flight calibration mode is run once per orbit. A systematic check is done as soon as the data arrive in the lab to verify that data remain within given limits. This did not lead to any unexplained alarm. More detailed analysis can be done – and will be done – to analyse how the experiment behaves after 12 yr (or more) of operation, being built for two years. An example of such a check is given on Fig. 7. This is the result of the analysis of the white noise which is sent by the onboard cal-box to the search coils, using the feedback wires of the search coils. On this step of the calibration mode, the strongest signal is sent. After a Fourier Transform of the signal, it is averaged in successive frequency bands to facilitate the verification. The power as a function of the frequency reflects the combined transfer functions of the search coils and of 10 Hz filter. On the figure two datasets are superimposed, one obtained at the beginning of the mission in 2001 and the other recently in 2012, in the same period of the year (same region of the magnetosphere). One can see the stability of the experiment behaviour with time.

4 STAFF sensitivity

The determination of the instrument magnetic sensitivity is an important issue in what concerns the validity of the scientific data analysis. As mentioned in the previous section, the instrument sensitivity is determined on the ground in the quiet site of Chambon-la-Forêt. An example is given in Fig. 8, on which has been superimposed to the ground determined sensitivity the results of measurements in space when in a region with no wave activity (lobes of the magnetosphere). The in flight data are for one spacecraft, (SC4) on one day. Data from STAFF-SA and from waveform in 10 and 180 Hz bands are over-plotted. The 10 and 180 Hz filter data cannot be simultaneous, but are close in time. Bz is plotted on top and Bx at bottom. One sees that in flight

CLUSTER STAFF search coils magnetometer calibration

P. Robert et al.

[Title Page](#)

[Abstract](#)

[Introduction](#)

[Conclusions](#)

[References](#)

[Tables](#)

[Figures](#)

[◀](#)

[▶](#)

[◀](#)

[▶](#)

[Back](#)

[Close](#)

[Full Screen / Esc](#)

[Printer-friendly Version](#)

[Interactive Discussion](#)



CLUSTER STAFF
search coils
magnetometer
calibration

P. Robert et al.

[Title Page](#)[Abstract](#)[Introduction](#)[Conclusions](#)[References](#)[Tables](#)[Figures](#)[⏪](#)[⏩](#)[◀](#)[▶](#)[Back](#)[Close](#)[Full Screen / Esc](#)[Printer-friendly Version](#)[Interactive Discussion](#)

STAFF-SC data are as good as on ground. For STAFF-SA output, the sensitivity is rather under estimated, the in flight experimental noise being below the ground sensitivity curve. This could be explained by the absence in flight of the 50 Hz power line signal and its harmonics seen on ground. Nevertheless a few interferences are seen, at 70, 140 and 280 Hz, internal to STAFF-SA, and at 900 Hz, coming from the DWP clock. When looking at the background noise for the 180 Hz waveform, one sees some thin interference lines, the frequency of which varies from time to time and from one spacecraft to another. This may limit the sensitivity of the measurements in the higher frequency range. The increase of the noise level at, and above, 10 Hz (180 Hz) comes from the cut-off frequencies of the filters. Due to the effect of the spin signal (see below), the noise level is higher on Bx than on Bz (parallel to the spin axis) at low frequency.

Figure 9 intends to show the possible evolution of the noise level with time. The spectra are obtained up to 9 Hz by 10 Hz low pass filter wave form data and above come from STAFF-SA. Data are averaged over one hour, taken in quiet periods in the same region for the four periods, in the Earth lobes. Data for spacecraft 1 to 4 are plotted from top to bottom, with Bx components at left and Bz ones at right. By being similar to Bx, it is not shown. One can notice the rather stable level with time, with nevertheless some increase for the A frequency band of STAFF-SA (8–64 Hz). The higher level at low frequency ($f < 0.3$ Hz) is due to an effect of the local spin signal (high level of DC magnetic field).

5 Sensor rotation and coordinate systems

To transform telemetry data into significant physical units we need to convert the data from the sensor coordinate system into one or another system, and in particular to transform from the spinning system into a fixed one, with respect to Sun and Earth for instance. For the waveform data, all transformations are done on ground, whereas for STAFF-SA data, part of the transformation is done on board. The following sections

are dedicated to define all intermediate coordinate systems required for this operation. Notice that these definitions can be used for other experiment of the same type, on any other mission.

All transformation matrices are named as: A_to_B where A and B are two different coordinate systems. To convert a vector given in the A system to the same vector expressed in the B system, the following expression is used:

$$\begin{pmatrix} x \\ y \\ y \end{pmatrix}_B = A_to_B \begin{pmatrix} x \\ y \\ y \end{pmatrix}_A$$

For general computation of this kind of matrix, see Robert (1993, 2003, 2004).

5.1 The Sensor Coordinate System (SCS)

This is the system where the original signal is measured (see Fig. 1). This system could be a non perfect orthogonal system (see Sect. 3.1)

5.2 The Orthogonal Sensor System (OSS)

This is a Cartesian orthogonal coordinate system. The original sensor system can be a non orthogonal system, the first step is to transform the data vector in an orthogonal coordinate system; Z axis being the reference of the new Orthogonal Sensor System. The corresponding matrix, called “SCS_to_OSS”, close to a unit matrix, is required and must be applied; values are supposed to be constant in time. Nevertheless, in a first time, taking into account the low deviation of the sensor to an orthogonal system for CLUSTER/STAFF ($\sim 0.2^\circ$, see Sect. 3.1), this correction is not applied and the matrix is set to unity matrix.

$$SCS_to_OSS \cong \begin{pmatrix} 1 & 0 & 0 \\ 0 & 1 & 0 \\ 0 & 0 & 1 \end{pmatrix}$$

[Title Page](#)

[Abstract](#)

[Introduction](#)

[Conclusions](#)

[References](#)

[Tables](#)

[Figures](#)

[⏪](#)

[⏩](#)

[◀](#)

[▶](#)

[Back](#)

[Close](#)

[Full Screen / Esc](#)

[Printer-friendly Version](#)

[Interactive Discussion](#)



5.3 The Data Sensor System (DSS)

The Body Build System (BBS, see next section) is a system fixed to the geometry of the spacecraft, and is used as the spacecraft system reference for all the experiments. Generally, for most of spacecraft missions, the Z axis is close to the maximum principal inertia axis also called the spin axis (for spin stabilized spacecraft). Nevertheless, for CLUSTER, this axis has been defined as the X axis (see Fig. 1).

In all our data, the convention taken is $Z = \text{spin axis}$. It means that we have an intermediate coordinate system, called Data Sensor System (DSS) which corresponds to the previous OSS, but where the axes are permuted, to make Z close to the spin axis.

By respect to the Fig. 1, $X_{\text{OSS}}, Y_{\text{OSS}}, Z_{\text{OSS}}$, becomes Y, Z, X in DSS.

This permutation is obtained by the following matrix:

$$\text{OSS_to_DSS} = \begin{pmatrix} 0 & 1 & 0 \\ 0 & 0 & 1 \\ 1 & 0 & 0 \end{pmatrix}$$

5.4 The Body Build System (BBS)

In the case of CLUSTER, the Z axis of the Data Sensor System is close to the X axis of the BBS system, but the misalignment angle is not easy to determine. It is also true for the small angle between this X_{BBS} and the true spin axis (precession and nutation motions). Nevertheless, an estimate of the cumulative angle is done in Sect. 5.5. Here, we neglect this small misalignment and assume $Z_{\text{DSS}} = X_{\text{BBS}}$. In all cases, 2 other axis may be rotated by an important angle (see Fig. 1). The corresponding matrix is required, called "DSS_to_BBS"; values are supposed to be constant. Practically, for the STAFF search coils of CLUSTER, this matrix is a rotation matrix of $\alpha = 45^\circ$.

CLUSTER STAFF
search coils
magnetometer
calibration

P. Robert et al.

[Title Page](#)
[Abstract](#)
[Introduction](#)
[Conclusions](#)
[References](#)
[Tables](#)
[Figures](#)
[⏪](#)
[⏩](#)
[◀](#)
[▶](#)
[Back](#)
[Close](#)
[Full Screen / Esc](#)
[Printer-friendly Version](#)
[Interactive Discussion](#)


$$\text{DSS_to_BBS} = \begin{pmatrix} 0 & 0 & 1 \\ \cos \alpha & -\sin \alpha & 0 \\ \sin \alpha & \cos \alpha & 0 \end{pmatrix}$$

5.5 The Spin Reference System (SRS)

The Spin Reference System has its Z axis parallel to the spin axis. This is a spinning system, rotating at the spin frequency. As mentioned above, there is a small misalignment between the X_{BBS} axis and the Z_{SCS} axis, as there is another slight misalignment between the X_{BBS} axis and the Z_{DSS} axis. This is not easy to separate the two angles, but it is possible to estimate the small angle between the Z_{SCS} axis and the true spin axis which define Z_{SRS} . This angle θ could be estimated by the measurement of the low spin signal on the ZSCS component.

If B_{xS}, B_{yS}, B_{zS} , are the amplitudes in nT of the spin sine on the three x, y, z components of the SCS system, this angle is estimated by:

$$\tilde{\theta} = \frac{B_{zS}}{\sqrt{B_{xS}^2 + B_{yS}^2 + B_{zS}^2}}$$

This angle could be constant, but can have also small variations during operations on the spacecraft (trajectory modifications, etc.). It has been estimated to an average value of $\sim 0.5\%$, and, in a first time, has not been taken into account. So, the “BBS_to_SRS” matrix is set to:

$$\text{BBS_to_SRS} \cong \begin{pmatrix} 0 & 1 & 0 \\ 0 & 0 & 1 \\ 1 & 0 & 0 \end{pmatrix}$$

This is a simple circular permutation.

5.6 The spin reference2 system (SR2)

The SR2 system, also called “SSS” for Spacecraft-SUN System, or “DS” for despun, is derived from the SRS system by a *despin* operation. The spinning Spacecraft is “stopped” just at the time where the X axis is in the plane containing the Z spin axis and the direction of the Sun. The rotation angle required is derived from the Sun pulse or any other quantity to compute the spin phase angle φ_s . This angle, and the corresponding time measurement, is required to build the “SRS_to_SR2” matrix. Terms of this matrix are fast varying with time. f_s is the spin frequency. The phase angle φ_s is calculated for each time tag of the data thanks to the Sun pulse signal. This gives:

$$\text{SRS_to_SR2} = \begin{pmatrix} \sin(2\pi f_s t + \varphi_s) & \cos(2\pi f_s t + \varphi_s) & 0 \\ \cos(2\pi f_s t + \varphi_s) & -\sin(2\pi f_s t + \varphi_s) & 0 \\ 0 & 0 & 1 \end{pmatrix}$$

5.7 The Geocentric Solar Ecliptic System (GSE)

The GSE system is a well known system, with the Z axis perpendicular to the Ecliptic plane, and the X axis toward the Sun. To do the transformation of the SSS to the GSE, the direction of the spin axis in the GSE system is required. Due to the gyroscopic effect of a spinning spacecraft, the spin axis is \sim constant in an inertial system, and so has a yearly variation in the GSE system, excepted during spacecraft operations.

SR2 to GSE transformation is done using module “tsr2gse” routine of ROCOTLIB software (see Robert, 1993, 2003, 2004). The Cartesian GSE coordinates of the direction of spin axis is required, as the corresponding time measurement. To transform spin right ascension and spin declination angle, given in STAFF-SC CAA data in Geocentric Equatorial Inertial system (GEI), routine “tgeigse” can be used. Those angles are also available in the auxiliary files available at CAA (latitude and longitude angles of the spin axis direction in GSE).

Note that in GSE system, each component mixes both parallel and perpendicular components to the spin axis. Because sensitivity is strongly different at low frequency

Title Page

Abstract

Introduction

Conclusions

References

Tables

Figures

⏪

⏩

◀

▶

Back

Close

Full Screen / Esc

Printer-friendly Version

Interactive Discussion



Assuming all small misalignment angles close to zero, we get:

$$[\text{BBS_to_SRS}][\text{DSS_to_BBS}] = \begin{pmatrix} \cos \alpha & -\sin \alpha & 0 \\ \sin \alpha & \cos \alpha & 0 \\ 0 & 0 & 1 \end{pmatrix}$$

Using expression of SRS_to_SR2 given in Sect. 5.6, with $\omega_s = 2\pi f_s$ after some calculus we get:

$$\begin{pmatrix} x \\ y \\ z \end{pmatrix}_{\text{SR2}} = \begin{pmatrix} \sin(\omega_s t + \varphi_s + \alpha) & \cos(\omega_s t + \varphi_s + \alpha) & 0 \\ \cos(\omega_s t + \varphi_s + \alpha) & -\sin(\omega_s t + \varphi_s + \alpha) & 0 \\ 0 & 0 & 1 \end{pmatrix} \begin{pmatrix} x \\ y \\ z \end{pmatrix}_{\text{DSS}}.$$

By neglecting all the small misalignment angles, the transformation from the Data Sensor System to the fixed SR2 system is simply reduced to a rotation in the spin plane of the fast varying angle $\psi = (\omega_s t + \varphi_s + \alpha)$.

This simplification is used for CLUSTER/STAFF calibration, but cannot be used for spacecraft or rocket having precession or nutation, or a non constant direction of the spin axis. In this case, the full computation must be done.

6 STAFF-SC calibration method

6.1 Spectrum calibration in sensor frame

The STAFF-SC experiment is a waveform unit which delivers magnetic waveform $x(t)_{\text{Volt}}$ in the sensor reference frame SCS. Due to the non linearity of the transfer function, all components of this signal at various frequencies must be corrected both in amplitude and phase. So the signal delivered by the search-coil is:

$$x(t)_{\text{Volt}} = \int_{-fs/2}^{+fs/2} X(f)_{\text{nT}} \alpha(f) e^{2i\pi f t} df \quad (1)$$

[Title Page](#)

[Abstract](#)

[Introduction](#)

[Conclusions](#)

[References](#)

[Tables](#)

[Figures](#)

[⏪](#)

[⏩](#)

[◀](#)

[▶](#)

[Back](#)

[Close](#)

[Full Screen / Esc](#)

[Printer-friendly Version](#)

[Interactive Discussion](#)



where $X(f)$ is the spectrum of the true ambient signal, in nT, $\alpha(f)$ is the complex transfer function of the sensor in V/nT and $f_s/2$ is the upper detectable frequency in Hz.

In a first time, let's consider the calibration of a single spectrum:

After digital processing, f_s being then the sampling frequency, Eq. (1) becomes:

$$5 \quad X_{k(\text{Volt})} = \sum_{-N/2}^{N/2} X_n \alpha_n e^{2i\pi nk} \quad (2)$$

X_n is the Fourier transform of the real signal $x(tk)$, in nT, to be estimated. The spectral resolution is $\delta f = f_s/N$.

So, to retrieve the original spectra (in nT) a simple Fourier transform is required:

$$X_n = \frac{1}{\alpha_n} \frac{1}{N} \sum_{-N/2}^{N/2} x_k e^{-2i\pi nk} \quad (3)$$

10 This is the theory. In practice, the original x_k signal is formed by a large sine signal at the spin frequency f_{spin} (~ 0.25 Hz), due to the rotation of the sensors into a large DC field (~ 100 nT), and the fluctuations (a few nT) are superimposed. So the amplitude of the “useful” frequency range is ~ 100 times less intense than the DC field (spin signal at ~ 0.25 Hz, see Fig. 10). Furthermore, a Fourier transform assumes a periodic signal
 15 of period N , and thus introduces large discontinuities on the edges of the window which generate meaningless high frequency components (see Robert, 1978, 1979).

Thus, the first step is to remove this large sine signal by a dedicated software, which compute the amplitude and phase of the sine for a given spin frequency, and remove it. Note that this measurement of amplitude and phase on the two B_x and B_z DSS
 20 spinning components allows us to compute the two components in the spin plane of the DC field, by applying the complex coefficient of the transfer function at the spin frequency, taking into account the phase angle given by the Sun pulse time to convert results in a no-spinning frame system (see later). Then, to avoid discontinuities on the

**CLUSTER STAFF
 search coils
 magnetometer
 calibration**

P. Robert et al.

[Title Page](#)

[Abstract](#) [Introduction](#)

[Conclusions](#) [References](#)

[Tables](#) [Figures](#)

[⏪](#) [⏩](#)

[◀](#) [▶](#)

[Back](#) [Close](#)

[Full Screen / Esc](#)

[Printer-friendly Version](#)

[Interactive Discussion](#)



edge of the window, the second step is to apply a weighting function on the signal after centering on zero.

So, the estimate of the original spectrum (in nT) is computed by:

$$\tilde{X}_n = \frac{1}{\alpha_n} \frac{1}{N} \sum_{-N/2}^{N/2} x_k W_k e^{-2i\pi nk}$$

- 5 Before computing the estimate of the calibrated waveform $\tilde{X}_{k(nT)}$ we have now to study the successive coordinate systems used to convert the signal recorded by the sensors in a useful coordinate system.

6.2 Computing calibrated waveform in SR2 system

10 From Eq. (3) we can estimate the calibrated waveform in SCS system by an inverse FFT, as

$$\tilde{X}_{k(nT)} = \sum_{-N/2}^{N/2} \tilde{X}_n e^{2i\pi nk}$$

Afterward, the calibrated waveform in SR2 system is computed by applying successive coordinate system matrix defined in Sects. 5.1 to 5.6 ; practically, for CLUSTER/STAFF, we use the simplified equation given in Sect. 5.9 and we get:

$$15 \begin{pmatrix} \tilde{X}_k \\ \tilde{Y}_k \\ \tilde{Z}_k \end{pmatrix}_{\text{SR2}} = \begin{pmatrix} \sin(\omega_s t_k + \varphi_s + \alpha) & \cos(\omega_s t_k + \varphi_s + \alpha) & 0 \\ \cos(\omega_s t_k + \varphi_s + \alpha) & -\sin(\omega_s t_k + \varphi_s + \alpha) & 0 \\ 0 & 0 & 1 \end{pmatrix} \begin{pmatrix} \tilde{X}_k \\ \tilde{Y}_k \\ \tilde{Z}_k \end{pmatrix}_{\text{DSS}}$$

One remains that SCS and DSS differ only by a circular permutation (see Sects. 5.2 and 5.3).

CLUSTER STAFF search coils magnetometer calibration

P. Robert et al.

Title Page

Abstract

Introduction

Conclusions

References

Tables

Figures

⏪

⏩

◀

▶

Back

Close

Full Screen / Esc

Printer-friendly Version

Interactive Discussion



6.3 Computing calibrated spectrum in SR2 system

The previous waveform being calibrated and expressed in SR2 system, the complex spectra is simply given by the FFT of this calibrated waveform, as:

$$\tilde{X}_n = \frac{1}{N} \sum_{-N/2}^{N/2} x_k W_k e^{-2i\pi nk}$$

- 5 The weighting function can be freely chosen. For CLUSTER/STAFF CAA product, the previous trapeze is taken. The same operation is of course done for \tilde{Y}_n and \tilde{Z}_n .

6.3.1 Window effect

Due to the weighting function, the previous calibrated waveform is significant only around the center of the window. To enlarge this part, we generally use a weighting function the shape of which is a trapeze or a rounded trapeze represented on Fig. 11. We can see that only $\sim 7/8$ of the waveform is significant.

15 In normal use, the length of the window is about a few spin periods. At least one spin period is required to estimate amplitude and phase of the sine, and 2 or 3 spin periods allow a best estimate. Beyond of a few spin periods, the DC field could change significantly, and the spin tone estimate will be less accurate. A good compromise is between one and 4 spin periods to properly estimate DC field and remove spin tone.

6.3.2 Summary of the various steps done during spectrum calibration

20 Calibration of the telemetry data is done in successive steps, described below. At this level, the calibration is done on successive data windows, to obtain calibrated spectra as described above.

CLUSTER STAFF search coils magnetometer calibration

P. Robert et al.

[Title Page](#)

[Abstract](#)

[Introduction](#)

[Conclusions](#)

[References](#)

[Tables](#)

[Figures](#)

[⏪](#)

[⏩](#)

[◀](#)

[▶](#)

[Back](#)

[Close](#)

[Full Screen / Esc](#)

[Printer-friendly Version](#)

[Interactive Discussion](#)



Get waveform in Volts

Telemetry data are given in integer values (called TM counts) within [0–65 535] interval corresponding to Volt range of [–5, +5 V]. The value of 65 535 comes from the used sample words of 16 bits long. This step does simply the conversion as:

$$x(t_n)_{\text{Volt}} = [x(t_n)_{\text{TM}} \times 10/65535] - 5.$$

Selecting time length of the windows determines the Δt . $\Delta f = 1$ resolution of each spectrum.

This step is named: “Calibration step # 1: Volts, spinning sensor system, with DC field”.

10 Cleaning raw waveforms

This step consists to remove the high amplitude signal at spin frequency due to the S/C rotation into a high DC field. Indeed, the wave useful signal is very low (a few nT) compared to the high spin tone (a few nT up to ~ 5 –600 nT). Even if the transfer function coefficient in amplitude is small at spin frequency, the spin tone in Volt remains too high do to a correct Fast Fourier Transform (see Robert et al., 1979).

This step is named: “Calibration step # 2: Volts, spinning sensor system, without DC field”.

The independent calibration of the spin tone, both in amplitude and phase, on the two B_x and B_y components, allows the determination of the two components in the spin plane, which can be compared to same components measured by the FGM experiment.

Calibration of each component within a given window

At a first time the signal is centered, and then a light trapezoidal windowing is applied to reduce edges effect before applying the FFT. Next, in frequency domain, for each

[Title Page](#)

[Abstract](#)

[Introduction](#)

[Conclusions](#)

[References](#)

[Tables](#)

[Figures](#)

[⏪](#)

[⏩](#)

[◀](#)

[▶](#)

[Back](#)

[Close](#)

[Full Screen / Esc](#)

[Printer-friendly Version](#)

[Interactive Discussion](#)



CLUSTER STAFF
search coils
magnetometer
calibration

P. Robert et al.

[Title Page](#)

[Abstract](#)

[Introduction](#)

[Conclusions](#)

[References](#)

[Tables](#)

[Figures](#)

[⏪](#)

[⏩](#)

[◀](#)

[▶](#)

[Back](#)

[Close](#)

[Full Screen / Esc](#)

[Printer-friendly Version](#)

[Interactive Discussion](#)



frequency, the complex spectrum is divided by the complex transfer to get a calibration in amplitude and phase. Since the transfer function is close to zero for frequencies close to zero, a cut-off frequency is applied, generally fixed to 0.1 Hz. At last, an inverse Fourier transform is performed to return in time domain and get a calibrated waveform in the given window, always in Sensor Spinning System.

This step is named “Calibration step # 3: nTesla, spinning sensor system, without DC field”.

Get calibrated waveform in the fixed SR2 system

By applying the appropriate matrix given in Sect. 6, which requires spin phase computation, one gets the calibrated waveform in SR2 system.

This step is named “Calibration step # 4: nTesla, fixed SR2 system, without DC field”.

Add DC field values on X and Y

This is an optional step which allows comparison with FGM data, because one obtains, for the two X and Y components in the spin plane, both the DC field and the fluctuation.

This step is named “Calibration step # 5: nTesla, fixed SR2 system, with xy DC field”.

Get calibrated waveform in GSE system or others

This is an optional step. From step 4, waveforms can be easily converted in GSE system or others geocentric system (GSM, MAG, GEO...) by using the ROCOTLIB software (see Robert, 1993, 2003, 2004).

Remark: this method provides a calibrated waveform *only significant on the central part of the window*, and produces discontinuities at the edges of each window. So this method cannot be used to produce continuous calibrated waveforms (see Robert, 1979, 1983). The method used to produce continuous calibrated waveforms is described in the next section.

Nevertheless this method can be used to produce the estimate of the calibrated spectrum $\tilde{X}_{n(nT)}^{SR2}$ in SR2 system (see Sect. 6.3) by applying a simple Fourier transform. The main advantage is a low CPU time consuming.

6.4 Waveform continuous calibration method

6.4.1 Method chosen for CLUSTER

To obtain a continuous waveform, we have to repeat the previous operation by overlapping successive windows and keep the central points, as illustrated Fig. 12. The calibration is done on a window of N_{kern} TM points, which determines the frequency resolution of the intermediate calibrated spectrum, so, the accuracy of the calibration.

The calibration window is then shifted of N_{shift} points.

The number N_{kern} must be optimized in order to:

- Do a correct despin: the window duration must be enough long to have a good estimate of the spin tone, but not too long because the amplitude (and phase) of the spin tone is varying with time, DC field could change in both direction and amplitude. A good compromise is between 2 and ~ 10 spin periods. One period is the minimum to run the despin algorithm.
- Have a high enough frequency resolution: the window duration must be enough long to get a significant sampling of the transfer function and to get a good accurate calibration.

The number N_{shift} must be optimized in order to:

- Be the shortest possible, for instance 2 points corresponding to the summit of the weighting function in the window.
- Could be extended to reduce CPU time but quality will be reduced too. If the weighting function is not constant during the N_{shift} point centered on the window,

CLUSTER STAFF search coils magnetometer calibration

P. Robert et al.

[Title Page](#)

[Abstract](#)

[Introduction](#)

[Conclusions](#)

[References](#)

[Tables](#)

[Figures](#)

[⏪](#)

[⏩](#)

[◀](#)

[▶](#)

[Back](#)

[Close](#)

[Full Screen / Esc](#)

[Printer-friendly Version](#)

[Interactive Discussion](#)



**CLUSTER STAFF
search coils
magnetometer
calibration**

P. Robert et al.

Title Page

Abstract

Introduction

Conclusions

References

Tables

Figures

⏪

⏩

◀

▶

Back

Close

Full Screen / Esc

Printer-friendly Version

Interactive Discussion



a parasite line appears on the spectrograms at fsr/Nshift frequency (fsr being the sampling rate).

Tests show that the best result is obtained by using a Gaussian weighting function, and by shifting the windows from one to the next one by two points, saving at each time the two central points at the summit of the Gaussian.

For the CLUSTER/STAFF-SC CWF CAA production, the chosen values for Nkern and Nshift parameters are given in Table 1. These values have been chosen to process a calibration which works whatever the amplitude and the time variation of the DC field, in normal conditions. This is important, because we can see that by the choice of the calibration parameters, *the solution for calibration data is not unique*. For very particular conditions, these parameters can be adjusted to get a best quality of the calibration.

6.4.2 Other calibration method

The previous method, which is a deconvolution in frequency domain, can be summarized by:

$$X_{k(nT)} = \text{FFT}^{-1} \left\{ \frac{1}{\alpha_n} \text{FFT}(X_{k(\text{Volt})} W_k) \right\}$$

More recently, THEMIS mission also includes search-coils (Roux, 2008), and for the data processing we used the deconvolution in time domain (Le Contel et al., 2008), which can be summarized by:

$$X_{k(nT)} = (X_{k(\text{Volt})} W_k) \times A_k$$

where “x” is the convolution operator and A_k the impulse function of $\frac{1}{\alpha_n}$ i.e. $\text{FFT}^{-1} \left\{ \frac{1}{\alpha_n} \right\}$.

From Plancherel’s theorem, notice that the two expressions are equivalent:

$$\begin{cases} X(t_k) \times A(t_k) \Leftrightarrow X(f_n) \cdot \alpha(f_n) \\ X(t_k) \cdot W(t_k) \Leftrightarrow X(f_n) \times W(f_n) \end{cases}$$

We find again in this method the concept of Nkern and Nshift, with the same meaning, as the weighting function, and the need of “cleaning” the waveform by removing the spin tone before any other processing.

Comparison of the two methods has been done by applying the two different softwares on the same data set, and concludes to a good agreement. Details of these comparisons will be done in another paper. Note that the calibration software used for CLUSTER is written in Fortran90, while the calibration software used for THEMIS is written in IDL. In this last case the convolution operation has been done by the build-in IDL function “CONVOL” which is very efficient. So, the good agreement of the two results is a proof of the validity of these two programs, which is very important for validate archive data bases.

7 STAFF-SA spectrum analyser

STAFF-SA has 5 input channels connected to 5 sensors: 3 magnetic and 2 electric. An overview of the instrument is given in Fig. 13. It makes estimations of the auto and cross-spectral power density at 27 frequencies, arranged in 3 bands A, B, C which have their own Automatic Gain Control.

The separation into 3 bands is performed by the analog part of the receiver. The digital part performs the despin for the spin-plane components and makes a filtering in 9 narrower frequency bands. Then it calculates the cross-spectral matrix of the 5 components in amplitude and in phase. The AGC are fixed during the time of an analysis, time controlled by telecommand.

The different steps of the on board calculation can be seen on Fig. 14, and for more details on the onboard calculation, see Sect. 4.3 of Cornilleau-Wehrlin et al. (1997).

In order to calculate the cross-spectral matrix, the components that are in the spin plane are despun:

**CLUSTER STAFF
search coils
magnetometer
calibration**

P. Robert et al.

[Title Page](#)

[Abstract](#)

[Introduction](#)

[Conclusions](#)

[References](#)

[Tables](#)

[Figures](#)

[⏪](#)

[⏩](#)

[◀](#)

[▶](#)

[Back](#)

[Close](#)

[Full Screen / Esc](#)

[Printer-friendly Version](#)

[Interactive Discussion](#)



$$Bu = By \cos(m) + Bz \sin(m)$$

$$Bv = Bz \cos(m) - By \sin(m)$$

where m is the instantaneous angular position of the spacecraft as derived from the on-board Sun Reference Pulse (SRP), and u and v are the fixed coordinates corresponding to the position of the STAFF search coil antennas (SCS) at the time of the Sun Pulse (i.e. when the SRP sees the SUN, see Fig. 1). Then the angle between this reference frame and the SR2 reference frame is $45 - 26.2 = 18.8^\circ$.

The calibration model that is applied on ground to the raw spectral matrix data is a combination of mathematical algorithms and tables of coefficients ($S(\text{AGC}), D(\text{AGC}), \tilde{S}(\text{Freq}), \tilde{D}(\text{Freq})$) used by those algorithms. The set of coefficients comes from measurements performed in the laboratory. The spin-plane receivers are strapped together in pairs with common AGC outputs. The calibration model will treat the sum and the difference of the both receivers. It is convenient to assume that the frequency-dependent and the AGC-dependent variations of the analogue transfer function can be separated.

The functions S and D take account of the variation with AGC level, assumed to be the same for all frequencies within any given band. The parameters S characterise the analog receivers; the mean spectral noise density in the overall pre-converter passband of analogue receiver m is a function of the corresponding AGC output A .

The functions \tilde{S} and \tilde{D} allow for the variation with frequency within each digital input channel. The parameters \tilde{S} characterise the bandpass of the digital spectrum analyser and also the variation with frequency of the analog receivers. They allow independent auto and cross-spectral estimates to be obtained in both amplitude and phase at each of the nine frequencies f .

Normally, when the AGC is locked and not saturated, for different levels of white noise, the variations of the autocorrelations with the frequencies must be the same. To calculate \tilde{S} and \tilde{D} , we have chosen a reference noise level corresponding to AGC = 80 (AGC = 0 to 255). Δ_{jj}^{mn} is a small correction which is not zero

CLUSTER STAFF
search coils
magnetometer
calibration

P. Robert et al.

[Title Page](#)[Abstract](#)[Introduction](#)[Conclusions](#)[References](#)[Tables](#)[Figures](#)[⏪](#)[⏩](#)[◀](#)[▶](#)[Back](#)[Close](#)[Full Screen / Esc](#)[Printer-friendly Version](#)[Interactive Discussion](#)

- if the spin rate is not nominal and/or
- if the spin-plane receivers are not identical

(with a set of parameters using D different of zero).

To calculate $\langle \vec{x}_i \vec{x}_j^* \rangle$, we use an iterative numerical method with a convergence test to stop the calculation. Note that we have assumed the variation of autocorrelations with the AGC level to be the same for all frequencies, within any given band; this is not entirely true for some frequencies and it can explain some small anomalies.

The last operation is to transform the data that are in a non standard fixed reference frame into SR2. For the components that are in the S/C spin plane a rotation of delta $\varphi = -18.8^\circ$ has to be applied, as well as a BBS to SRS rotation matrix to have B_z parallel to the spin axis (see Sect. 5).

8 STAFF-SC/STAFF-SA continuity and other cross-check

Once the transfer function is calculated, one of the first checks is to compare the results of the data analysis by the two STAFF sub experiments. Both continuity in the spectra and similarity in the wave characterisation results have been checked.

8.1 Power spectra

For this purpose we have used a special mode of operation which allows to maximize the frequency overlap between the two experiments, between 8 Hz and 180 Hz. Example for different kinds of wave data are given below on Fig. 15. Two kinds of wave fluctuations are shown, for two different spacecraft. Only B_x and B_z components are shown. Whereas the overlap and continuity are rather good, one can be aware of some effect on STAFF-SA at lower frequencies, as reported in the CLUSTER STAFF CAA Calibration report (Robert et al., 2012).

[Title Page](#)

[Abstract](#)

[Introduction](#)

[Conclusions](#)

[References](#)

[Tables](#)

[Figures](#)

[⏪](#)

[⏩](#)

[◀](#)

[▶](#)

[Back](#)

[Close](#)

[Full Screen / Esc](#)

[Printer-friendly Version](#)

[Interactive Discussion](#)



8.2 Wave characteristics determination

It is important to determine the characteristics of measured waves which can be done by means of the three magnetic orthogonal sensors. The parameters that can be obtained at one point of measurements are in particular wave planarity, ellipticity, sense of polarization, propagation angle with respect to main magnetic field.

These quantities are obtained on ground for the wave form data up to either 10 Hz or 180 Hz depending on the telemetry mode, whereas the coefficient of the complex spectral matrix are onboard calculated by the STAFF-SA for the frequency range 8 Hz–4 kHz. Figure 16 give an example of such analysis performed by data coming from both waveform (left) and SA (right), observed by Cluster 1 close to the magnetopause on 26 March 2007. The color scale is the same for both data set analysis, but the frequency scale is different, linear for waveform data and log for SA. The top panel shows the dynamic spectra. Then different polarisation and propagation parameters are plotted in the time-frequency plane for only amplitudes greater than a minimum level (for PSD larger than $10^{-6} \text{ nT}^2 \text{ Hz}^{-1}$). Those parameters are the ellipticity of the emission, the propagation angle $\theta(k, B)$ and the azimuth angle ($\phi = 0$ indicates the spacecraft sun direction projected in the plane perpendicular to B). The three polarization parameters are computed through the singular value decomposition method (Santolík et al., 2003) using the PRASSADCO tool (Santolík, 2003)

The common frequency band between STAFF-SA and STAFF-SC is about 60–225 Hz. The main emission observed during that time interval is detected between 07:22:45 and 07:23:30 UT around 50 Hz and up to more than 200 Hz in the middle of the time interval. One can remark that the polarisation and propagation parameters calculated from the two data sets give the same results, in the limit of their respective frequency and time resolutions. During this event, the magnetic emissions were clearly right hand polarized; the theta angle was most of the time less than 45° , and the phi angle displays a nice rotation (from -90 , to -180 , 180 then to 90°). The similar values of the different parameters obtained from both parts of the experiment, together

CLUSTER STAFF search coils magnetometer calibration

P. Robert et al.

Title Page

Abstract

Introduction

Conclusions

References

Tables

Figures

⏪

⏩

◀

▶

Back

Close

Full Screen / Esc

Printer-friendly Version

Interactive Discussion



with physically “reasonable” results, give some confidence on the validity of the data processing performed. This kind of tests has been performed at the beginning of the mission in order to find an error in the rotation matrix, which has been solved since.

9 STAFF-SC/FGM comparisons

9.1 Interest of such study

The possibility to recover two DC magnetic field components by the search-coil experiment is particularly useful, because it allows a comparison with the result of the flux gate magnetometer experiment. It has already been done for the GEOS mission (see Jones, 1977), here the agreement found was $\sim 4\%$ on the magnitude and $\sim 4^\circ$ on the direction (Robert, 1979).

For CLUSTER the two STAFF and FGM experiments run successfully since the beginning of the mission. In the frame of the CAA Cross-calibration meeting, it was obvious to look after a comparison of the result of the two instruments in their common frequency range. It is not only useful to validate the data, but only to precise the respective use of the two instruments.

So, during all calibration meetings, from 2006 until now, the STAFF-FGM comparisons were day by day in progress. Thanks to this kind of comparison, we realised that the transfer function of the search-coils was underestimated (Robert, 2nd Cross Calibration Workshop, 2006). After investigation, it was identified that the shape of the calibration device (Helmholtz’ coils) was slowly distorted with time (see Sect. 3.2 and Robert, 14th Cross Calibration Workshop, 2011). New calibration tables were used, and the STAFF-FGM agreement improved.

CLUSTER STAFF search coils magnetometer calibration

P. Robert et al.

[Title Page](#)

[Abstract](#)

[Introduction](#)

[Conclusions](#)

[References](#)

[Tables](#)

[Figures](#)

[⏪](#)

[⏩](#)

[◀](#)

[▶](#)

[Back](#)

[Close](#)

[Full Screen / Esc](#)

[Printer-friendly Version](#)

[Interactive Discussion](#)



**CLUSTER STAFF
search coils
magnetometer
calibration**

P. Robert et al.

Title Page

Abstract

Introduction

Conclusions

References

Tables

Figures

◀

▶

◀

▶

Back

Close

Full Screen / Esc

Printer-friendly Version

Interactive Discussion

9.2 Data origin

FGM data are issued from CAA, in FULL resolution mode, in GSE system. They are converted into SR2 system to compare the spin plane components with STAFF-SC data.

5 Search-coil data are calibrated following the process described in Sect. 6.4, in NBR mode, and of course in SR2 system. Step 5, “nTesla, fixed SR2 system, with xy DC field” is used.

9.3 Direct waveform comparison

9.3.1 A typical event studied at various scale

10 The following results have been shown in different cross-calibration meeting. The 24 February 2001 case is interesting, because we can look at it at various time scales. Figure 17 shows a waveform comparison between 21:00 and 22:00 UT. The B_{\perp} component is computed from B_{xS} and B_{yS} components in the spin plane as:

$$B_{\perp} = \sqrt{B_{xS}^2 + B_{yS}^2}$$

15 While the direction, or phase φ is computed from:

$$\sin \varphi = B_{yS} / B_{\perp}$$

$$\cos \varphi = B_{xS} / B_{\perp}$$

On the B_{\perp} component, at a first glance, the agreement is good within around, with:

$$20 \frac{\Delta B_{\perp}}{B_{\perp}} = \frac{(B_{\perp}^{\text{STA}} - B_{\perp}^{\text{FGM}})}{(B_{\perp}^{\text{STA}} + B_{\perp}^{\text{FGM}}) / 2} \sim 4\%$$

while the phase angle difference is:

$$\Delta\varphi = (\varphi^{\text{STA}} - \varphi^{\text{FGM}}) \sim 5^\circ$$

After re-sampling the data to obtain the same sample rate on the two data sets, we can compute the mean difference point to point, and the result is much better:

$$\frac{\Delta B_{\perp}}{B_{\perp}} = 0.77\%$$

$$\sigma B_{\perp} = 0.84\%$$

If we make a zoom on the narrow spike between 21:56 and 21:58 UT (Fig. 18), we can see that the agreement is also good on short time scale ~ 2 mn. We find as previous

$$\frac{\Delta B_{\perp}}{B_{\perp}} < 1\%$$

$$\Delta\varphi \cong 3^\circ$$

9.3.2 Statistic over 10 yr on spin plane DC field

Figure 19 shows a statistics performed over 10 yr of STAFF-FGM DC field comparison. The 58 events altogether have been chosen, in four various conditions each year:

- low DC field, low ULF activity,
- low DC field, high ULF activity,
- high DC field, low ULF activity,
- high DC field, high ULF activity.

CLUSTER STAFF search coils magnetometer calibration

P. Robert et al.

[Title Page](#)

[Abstract](#)

[Introduction](#)

[Conclusions](#)

[References](#)

[Tables](#)

[Figures](#)

[⏪](#)

[⏩](#)

[◀](#)

[▶](#)

[Back](#)

[Close](#)

[Full Screen / Esc](#)

[Printer-friendly Version](#)

[Interactive Discussion](#)



Panel a shows the relative difference $\Delta B_{\perp}/B_{\perp}$ in %, where we can see that this difference is roughly constant for each spacecraft during the 10 yr studied.

Panel b shows the standard deviation of $\Delta B_{\perp}/B_{\perp}$ which is between 0.5 and 5%, except one point at 12%, but which correspond to a very low B_{\perp} , so $\Delta B_{\perp}/B_{\perp}$ become relatively high taking into account the accuracy of the measurement.

Panel c shows the amplitude of the $B_{\perp DC}$ field for each event, from a few nT to 500 nT.

At last, panel d gives the phase difference of the B_{\perp} component in SR2 system.

Concerning the relative stability of $\Delta B_{\perp}/B_{\perp}$, we can see that it is independent of the magnitude of the DC field, whatever the level of ULF activity. Furthermore, for each spacecraft, this difference remains constant all over the ten years study. This is an important result, because it shows that the transfer function remains constant from the beginning of the mission until 10 yr after. This result could be confirmed by a dedicated study of the onboard calibration signals.

Another important result is the difference from one spacecraft to another: in fact, the best result seems be obtained for the S/C #1, where the transfer function has been obtained by the averaging of the 3 others (S/C2, S/C3 and S/C4). This result is thus directly directed by the estimate of the transfer function on the ground, and gives an estimate of their accuracy (see Sect. 3). The choice has been done to keep each of the 3×4 transfer function slightly different, but, as these tables should be all theoretically identical, another choice could have been to set all tables to the S/C#1 average table.

Concerning the direction, most of the time this $\Delta\varphi$ difference is between 2 and 4°. Nevertheless, for some cases, this difference changes of sign, and is between -2 to -4°. This change is not explained up to now.

9.3.3 Comparison at 1 Hz

Figure 20 shows an event with an almost monochromatic wave at low frequency (~ 1 Hz) superimposed to a low DC variation. On the left part, one can see a constant difference of $\sim 1\%$ on the B_{\perp} component, as expected, and a phase difference of

[Title Page](#)

[Abstract](#)

[Introduction](#)

[Conclusions](#)

[References](#)

[Tables](#)

[Figures](#)

[⏪](#)

[⏩](#)

[◀](#)

[▶](#)

[Back](#)

[Close](#)

[Full Screen / Esc](#)

[Printer-friendly Version](#)

[Interactive Discussion](#)



~ 4°. The zoom (on right part) shows still the same agreement on the DC part, both in amplitude and phase. To see a more precise comparison for the component at 1 Hz, we shift the FGM data of 3.3 nT (1.1 %) to have a better superimposition of the two curves (Fig. 21). The result is rather satisfying, a good fit being found at a first glance, but a spectral analysis is required to get a best estimate of the difference (see Sect. 9.4.1).

9.3.4 Comparison at 6 Hz

The following example corresponds to another almost monochromatic wave at ~ 6 Hz, always superimposed to a low DC variation (Fig. 22). The wave occurs at ~ 09:39 UT on *By*. Agreement on DC files remains the same ($\Delta B/B < 1\%$, $\Delta\phi \sim 3^\circ$).

By zooming on the wave (Fig. 23) we can identify a ~ 6 Hz wave whose both amplitude and phase seems to be in good agreement, but as previously, a spectral analysis is required to get more details (see Sect. 9.4.2).

9.4 Spectrum comparison

9.4.1 STAFF-SC/FGM sensitivity

Figure 24 shows a spectrum of STAFF and FGM done during a very quiet period, which means that these two curves can be considered as the sensitivity of the two instruments. The two curves cross at ~ 0.7 Hz, that is to say that at this frequency the two instruments have the same sensitivity. Below 0.7 Hz, FGM is not only more sensitive, but gives of course the three components of the DC field contrary to STAFF. Above 0.7 Hz, the search-coils are more sensitive and can detect event of smaller magnitude. This leads to choose one experiment rather than the other, according to whether you look at DC or at waves, and for waves to which frequency range you want to focus on. In fact the two experiments are quite complementary.

[Title Page](#)

[Abstract](#)

[Introduction](#)

[Conclusions](#)

[References](#)

[Tables](#)

[Figures](#)

[⏪](#)

[⏩](#)

[◀](#)

[▶](#)

[Back](#)

[Close](#)

[Full Screen / Esc](#)

[Printer-friendly Version](#)

[Interactive Discussion](#)



~ 4 Hz, the agreement is very good. It evidences the complementarity of both experiments permitting to analyse a wide frequency range with a good precision.

9.4.5 Doppler Effect on sensitivity

Classical spectra are computed in the fixed (not spinning) system, as shown in Fig. 29, where we chose an event corresponding to the background noise. Ground sensitivity is plotted in black. Only the Z component (blue curve) is not disturbed by the spin. But the X and Y components (red and green curves respectively), in the spin plane, suffer of the Doppler Effect: the large peak at spin frequency (0.25 Hz) corresponds to the 0. Hz frequency in the spinning system of the sensor, and thus could lead to an infinite value since the transfer function at this frequency is null. Practically, to avoid an undefined value, one chooses a very low value rather than 0.

The two holes on X and Y at 0.25 ± 0.1 Hz correspond to the cut off frequency chosen during the calibration (see Sect. 6). Furthermore, the spin effect added with the Doppler Effect leads to decrease the sensitivity on X and Y components.

In other words, because the transfer function is close to zero at $f = 0$, which means that a right-handed polarized wave at spin frequency in the spinning coordinate system *cannot be recorded* by the STAFF sensor (see Fig. 30). Indeed, it is seen at $f = 0$ by the sensor, so the search-coils does not provide any signal at this frequency. For this right wave,

$$f_{SR} = f_{SR2} - f_{spin}$$

On the other hand, a *left*-handed polarized wave at any frequency, including DC, is recorded by the STAFF sensor. For this left wave,

$$f_{SR} = f_{SR2} + f_{spin}$$

This also means that, at low frequency, we *cannot* expect a full agreement between STAFF and FGM, except for left-handed polarized wave. But for frequencies $f \gg f_{spin}$ as we find previously, there is a good agreement.

CLUSTER STAFF search coils magnetometer calibration

P. Robert et al.

Title Page

Abstract

Introduction

Conclusions

References

Tables

Figures

◀

▶

◀

▶

Back

Close

Full Screen / Esc

Printer-friendly Version

Interactive Discussion



CLUSTER STAFF
search coils
magnetometer
calibration

P. Robert et al.

[Title Page](#)[Abstract](#)[Introduction](#)[Conclusions](#)[References](#)[Tables](#)[Figures](#)[⏪](#)[⏩](#)[◀](#)[▶](#)[Back](#)[Close](#)[Full Screen / Esc](#)[Printer-friendly Version](#)[Interactive Discussion](#)

To well understand the consequences of the Doppler Effect with a non-linear transfer function, Fig. 31 shows this spectrum in the SR spinning coordinate. The peak at the spin frequency corresponds now to the DC magnetic field, and the cut-off frequency looks the same for the 3 *XYZ* components. Moreover, we can see that beyond twice spin frequency, the sensitivity becomes the same on the three components, that is not the case in fixed SR2 system.

For more details on the Doppler Effect on detected waves, see Robert et al. (1978, 1979) and Robert (1979).

10 Conclusions

A method to calibrate the waveform delivered by a rotating search coil has been proposed, and used for CLUSTER/STAFF-SC data. It has been shown that the solution to waveform calibration data is not unique and depends of the signal itself. Various coordinate systems required to transform telemetry data to a fixed and known coordinate system have been defined. Method and coordinate systems defined here can be used for another mission of same kind. This paper shows also that quality of the transfer functions of the instrument is a key to get best accurate calibrated waveforms and spectra. Sampling and transfer function determine the sensitivity of the instrument, which has been established both from the calibrated waveform issued from STAFF-SC and for the calibrated spectra issued from STAFF-SA. It has been shown that we get a good continuity between the two sub-instruments, into their common frequency range.

Cross calibration between STAFF-SC in normal mode (0–10 Hz) and FGM in the same frequency range leads to an agreement $\sim \pm 1\%$ on the DC field in the spin plane and within a few % between 0.5 and 10 Hz. The respective sensitivity of the two instruments, deduced from observations done during a period of a very quiet magnetic activity, shows the two curves crossing at 0.7 Hz. Below this frequency, the fluxgate is more sensitive and gives the three components of the DC field. Above this frequency, the search coil is more sensitive.

Statistic study of the DC field, as measured by FGM and by STAFF at spin frequency, over ten years shows a constant difference between the two instruments, and so demonstrates the stability of the quality of measurements performed by both instruments.

5 *Acknowledgements.* The authors deeply thank A. Balogh, first PI of FGM experiment, and the following ones, E.A. Lucek and C. Carr, and the whole FGM team who has contributed to deliver to the CAA an invaluable set of data available to the scientific community.

10 All engineers who have been working on the STAFF data since the beginning of the mission, too numerous to be mentioned, are fully thanked. The authors are indebted to Christophe Coillot for establishment of the corrective transfer function formula, and Bertrand de la Porte for the test on the transfer function.

Many thanks to the CAA itself for its action, and for the organization of a long series of cross-calibration meetings from which a large part of this work is issued.

STAFF instrumentation and part of data analysis have got support from ESA and CNES.

15 References

Balogh, A., Dunlop, M. W., Cowley, S. W. H., Southwood, D. J., Thomlinson, J. G., Glassmeier, K. H., Musmann, G., Lühr, H., Buchert, S., Acuña, M. H., Fairfield, D. H., Slavin, J. A., Riedler, W., Schwingenschuh, K., and Kivelson, M. G.: The cluster magnetic field investigation, *Space Sci. Rev.*, 79, 65–91, 1997.

20 Balogh, A., Carr, C. M., Acuña, M. H., Dunlop, M. W., Beek, T. J., Brown, P., Fornacon, K.-H., Georgescu, E., Glassmeier, K.-H., Harris, J., Musmann, G., Oddy, T., and Schwingenschuh, K.: The Cluster Magnetic Field Investigation: overview of in-flight performance and initial results, *Ann. Geophys.*, 19, 1207–1217, doi:10.5194/angeo-19-1207-2001, 2001.

25 Cornilleau-Wehrin, N., Chauveau, P., Louis, S., Meyer, A., Nappa, J. M., Perraut, S., Rezeau, L., Robert, P., Roux, A., de Villedary, C., de Conchy, Y., Friel, L., Harvey, C. C., Hubert, D., Lacombe, C., Manning, R., Wouters, F., Lefeuvre, F., Parrot, M., Pinçon, J. L., Poirier, B., Kofman, W., and Louarn, P.: The CLUSTER Spatio-Temporal Analysis of Field Fluctuations (STAFF) Experiment, *Space Sci. Rev.*, 79, 107–136, 1997.

CLUSTER STAFF search coils magnetometer calibration

P. Robert et al.

[Title Page](#)

[Abstract](#)

[Introduction](#)

[Conclusions](#)

[References](#)

[Tables](#)

[Figures](#)

[⏪](#)

[⏩](#)

[◀](#)

[▶](#)

[Back](#)

[Close](#)

[Full Screen / Esc](#)

[Printer-friendly Version](#)

[Interactive Discussion](#)



**CLUSTER STAFF
search coils
magnetometer
calibration**

P. Robert et al.

[Title Page](#)[Abstract](#)[Introduction](#)[Conclusions](#)[References](#)[Tables](#)[Figures](#)[⏪](#)[⏩](#)[◀](#)[▶](#)[Back](#)[Close](#)[Full Screen / Esc](#)[Printer-friendly Version](#)[Interactive Discussion](#)

Cornilleau-Wehrlin, N., Chanteur, G., Perraut, S., Rezeau, L., Robert, P., Roux, A., de Villedary, C., Canu, P., Maksimovic, M., de Conchy, Y., Hubert, D., Lacombe, C., Lefeuvre, F., Parrot, M., Pinçon, J. L., Décréau, P. M. E., Harvey, C. C., Louarn, Ph., Santolik, O., Alleyne, H. St. C., Roth, M., Chust, T., Le Contel, O., and STAFF team: First results obtained by the Cluster STAFF experiment, *Ann. Geophys.*, 21, 437–456, doi:10.5194/angeo-21-437-2003, 2003.

Cross Calibration Workshops: The purpose of the cross-calibration workshops is to provide a forum where observations from different Cluster instruments are compared in detail, presentations of organized workshops between September 2005 and March 2013, available at: ftp://ftp.lpp.polytechnique.fr/robert/keep/Biblio_et_CV/ESA_CrossCal_Meetings, 1st CrossCal Workshop, ESTEC, 2–3 February 2006/CrossCal01-STAFF_Robert.ppt, 2nd CrossCal Workshop, ESTEC, 16 May 2006/CrossCal02-STAFF_Robert.ppt, 8th CrossCal Workshop, Kinsale, Co. Cork, Ireland, 28–30 October 2008/CrossCal08-STAFF_Robert.ppt 9th CrossCal Workshop, Jesus College, Cambridge, 23–27 March 2009/CrossCal09-STAFF_Burlaud.ppt, 10th CrossCal Workshop, L'Observatoire de Paris, Paris, 3–4 November 2009/CrossCal10-STAFFActions_Burlaud.ppt/CrossCal10-STAFF-SA_De_Conchy.ppt/CrossCal10-STAFF-SC_Robert.ppt, 11th CrossCal Workshop, Hotel die Tanne, Goslar, 7–9 April 2010/CrossCal11-STAFF_Burlaud.ppt,/CrossCal11-STAFF_Robert.ppt, 12th CrossCal Workshop, CESR, Toulouse, 26–28 October 2010/CrossCal12-STAFF_Cornilleau.ppt, /CrossCal11-STAFF_Robert.ppt, 13th CrossCal Workshop, IRF, Uppsala, Sweden, 13–15 April 2011/CrossCal13-STAFF_Robert.ppt, 14th CrossCal Workshop, York, UK, 5–7 October 2011/CrossCal14-STAFF_Robert.ppt/CrossCal14-STAFF_Santolik.ppt, 15th CrossCal Workshop, University College of London, London, 17–19 April 2012/CrossCal15-STAFF_Robert_Piberne.pptx, 16th CrossCal Workshop, Toulouse, France, 6–9 November 2012/CrossCal16-STAFF_Robert_Piberne.ppt, 17th CrossCal Workshop, ESOC, Darmstadt, Germany, 25–27 March 2013/CrossCal17-STAFF_Piberne.ppt, 18th CrossCal Workshop, Cosener's House, Abingdon, UK, 23–25 October 2013/CrossCal18-STAFF_Piberne.pptx.

Gurnett, D. A., Huff, R. L., and Kirchner, D. L.: The wide-band plasma wave investigation, *Space Sci. Rev.*, 79, 195–208, 1997.

**CLUSTER STAFF
search coils
magnetometer
calibration**

P. Robert et al.

[Title Page](#)
[Abstract](#)[Introduction](#)[Conclusions](#)[References](#)[Tables](#)[Figures](#)[⏪](#)[⏩](#)[◀](#)[▶](#)[Back](#)[Close](#)[Full Screen / Esc](#)[Printer-friendly Version](#)[Interactive Discussion](#)

- Gustafsson, G., Boström, R., Holback, B., Holmgren, G., Lundgren, A., Stasiewicz, K., Ahlén, L., Mozer, F. S., Pankow, D., Harvey, P., Berg, P., Ulrich, R., Pedersen, A., Schmidt, R., Butler, A., Fransen, A. W. C., Klinge, D., Thomsen, M., Fälthammar, C. G., Lindqvist, P. A., Christenson, S., Holtet, J., Lybekk, B., Sten, T. A., Tanskanen, P., Lappalainen, K., and Wygant, J.: The electric field and wave experiment for the Cluster mission, *Space Sci. Rev.*, 79, 137–156, 1997.
- Jones, D.: Introduction to the S-300 wave experiment onboard GEOS, *Space Sci. Rev.*, 22, 327–332, 1977.
- Knott, K.: Payload of the GEOS scientific geostationary satellite, *ESA Sci. Tech. Rev.*, 1, 173–196, 1975.
- Le Contel, O., Roux, A., Robert, P., Coillot, C., Bouabdellah, A., de la Porte, B., Alison, D., Ruocco, S., Angelopoulos, V., Bromund, K., Chaston, C. C., Cully, C., Auster, H. U., Glassmeier, K. H., Baumjohann, W., Carlson, C. W., McFadden, J. P., and Larson, D.: First results of the THEMIS Search Coil Magnetometers, *Space Sci. Rev.*, 141, 509–534, doi:10.1007/s11214-008-9371-y, 2008.
- Nykyri, K., Grison, B., Cargill, P. J., Lavraud, B., Lucek, E., Dandouras, I., Balogh, A., Cornilleau-Wehrin, N., and Rème, H.: Origin of the turbulent spectra in the high-altitude cusp: Cluster spacecraft observations, *Ann. Geophys.*, 24, 1057–1075, doi:10.5194/angeo-24-1057-2006, 2006.
- Paschmann, G., Melzner, F., Frenzel, R., Vaith, H., Parigger, P., Pagel, U., Bauer, O. H., Haerendel, G., Baumjohann, W., Scopke, N., Torbert, R. B., Briggs, B., Chan, J., Lynch, K., Morey, K., Quinn, J. M., Simpson, D., Young, C., McIlwain, C. E., Fillius, W., Kerr, S. S., Mahieu, R., and Whipple, E. C.: The electron drift instrument for cluster, *Space Sci. Rev.*, 79, 233–269, 1997.
- Pedersen, A., Cornilleau-Wehrin, N., de la Porte, B., Roux, A., Bouabdellah, A., Décréau, P. M. E., Lefeuvre, F., Sené, F. X., Gurnett, D., Huff, R. R., Gustafsson, G., Holmgren, G., Woolliscroft, L. J. C., Thompson, J. A., and Davies, P. H. N.: The Wave Experiment Consortium (WEC), *Space Sci. Rev.*, 79, 93–106, 1997.
- Perry, C., Eriksson, T., Escoubet, P., Esson, S., Laakso, H., McCaffrey, S., Sanderson, T., and Bowen, H.: The ESA Cluster Active Archive, in: Proceedings of the Cluster and Double Star Symposium 5th Anniversary of Cluster in Space, ESTEC, Noordwijk, 2005.

CLUSTER STAFF
search coils
magnetometer
calibrationP. Robert et al.

[Title Page](#)[Abstract](#)[Introduction](#)[Conclusions](#)[References](#)[Tables](#)[Figures](#)[◀](#)[▶](#)[◀](#)[▶](#)[Back](#)[Close](#)[Full Screen / Esc](#)[Printer-friendly Version](#)[Interactive Discussion](#)

Pinçon, J. L. and Lefeuvre, F.: Local characterization of homogeneous turbulence in a space plasma from simultaneous measurements of field components at several points in space, J. Geophys. Res., 96, 1789–1802, 1991.

5 Robert, P.: Intensité et polarisation des ondes UBF détectées à bord de GEOS-1, Méthode d'analyse numérique du signal et production en routine de sommaires expérimentateurs, Problèmes rencontrés et solutions pratiques, Note Technique CRPE/EET/71, May, available at: ftp://ftp.lpp.polytechnique.fr/robert/keep/Biblio_et_CV/Working_documents/1979_Robert_NTCRPE71_Intensite_et_Polarisation_des_ondes_UBF.pdf (last access: 4 December 2013), 1979a.

10 Robert, P.: Measurement by the S-300 experiment of two components of the DC magnetic field, in the X–Y plane of the satellites GEOS-1 and GEOS-2, Comparison with the results of the S-331 magnetometer, Document de Travail CRPE/EET, July, available at: ftp://ftp.lpp.polytechnique.fr/robert/keep/Biblio_et_CV/Working_documents/1979_Robert_DTCRPE_Measurement_by_S300_of_2comp_DC_field.pdf (last access: 3 December 2013), 1979b.

15 Robert, P.: Cluster software tools – Part I: Coordinate transformations library, Document de Travail, DT/CRPE/1231, July, available at: ftp://ftp.lpp.polytechnique.fr/robert/keep/Biblio_et_CV/Working_documents/1993_Robert_DTCRPE1231_ROCOTLIB.pdf (last access: 3 December 2013), 1993.

20 Robert, P.: ROCOTLIB: a rather complete suite of coordinate transformation routines, Issue 1, Rev. 8, November 2003, available at: <http://cdpp.eu/index.php/Scientific-libraries/rocotlib.html> (last access: 3 December 2013), 2003.

Robert, P.: ROCOTLIB: a coordinate Transformation Library for Solar-Terrestrial studies, & french version, ROCOTLIB: une bibliothèque de changement de coordonnées pour les études Soleil-Terre, Le Bulletin du Centre de Données de la Physique des Plasmas Num. 8t, CNES, 2004.

25 Robert, P., Kodera, K., Perraut, S., Gendrin, R., and de Villedary, C.: Polarization characteristics of ULF waves detected onboard GEOS-1, Problems encountered and practical solutions, XIXth URSI General Assembly, Helsinki, Finland, 31 July–8 August, available at: ftp://ftp.lpp.polytechnique.fr/robert/keep/Biblio_et_CV/Publications/1978_Robert_URSI_Helsinki.pdf (last access: 3 December 2013), 1978.

30

**CLUSTER STAFF
search coils
magnetometer
calibration**

P. Robert et al.

[Title Page](#)

[Abstract](#)

[Introduction](#)

[Conclusions](#)

[References](#)

[Tables](#)

[Figures](#)

[⏪](#)

[⏩](#)

[◀](#)

[▶](#)

[Back](#)

[Close](#)

[Full Screen / Esc](#)

[Printer-friendly Version](#)

[Interactive Discussion](#)



Robert, P., Kodera, K., Perraut, S., Gendrin, R., and de Villedary, C.: Amplitude et polarisation des ondes UBF détectées à bord du satellite GEOS-1, Méthodes d'analyse, problèmes rencontrés et solutions pratiques , Ann. Télécommun., 34, 179–186, 1979.

Robert, P., Burlaud, C., Maksimovic, M., Cornilleau-Wehrin, N., and Piberne, R.: Calibration Report of the STAFF Measurements in the Cluster Active Archive (CAA), Doc. No. CAA-STA-CR-002, issue 3.0, 16 May 2012, available at: http://caa.estec.esa.int/documents/CR/CAA_EST_CR_STA_v30.pdf (last access: 3 December 2013), 2012.

Roux, A., Le Contel, O., Robert, P., Coillot, C., Bouabdellah, A., de la Porte, B., Alison, D., Ruocco, S., and Vassal, M. C.: The search coil magnetometer for THEMIS, Space Sci. Rev., 141, 265–275, doi:10.1007/s11214-008-9455-8, 2008.

Santolik, O.: Propagation Analysis of STAFF-SA Data with Coherency Tests (a User's Guide to PRASSADCO), LPCE/NTS/073.D, Lab. Phys. Chimie Environ./CNRS, Orleans, France, available at: <http://aurora2.troja.mff.cuni.cz/~santolik/PRASSADCO/tc2/doc/guide.pdf> (last access: 3 December 2013), 2003.

Santolik, O., Parrot, M., and Lefeuvre, F.: Singular value decomposition methods for wave propagation analysis, Radio Sci., 38, 1010, doi:10.1029/2000RS002523, 2003.

Woolliscroft, L. J. C., Alleyne, H. S. C., Dunford, C. M., Sumner, A., Thompson, J. A., Walker, S. N., Yearby, K. H., Buckley, A., Chapman, S., Gough, M. P., and the DWP Co-investigators: The digital wave processing experiment on Cluster, Space Sci. Rev., 79, 209–231, 1997.

GID

3, 679–751, 2013

CLUSTER STAFF search coils magnetometer calibration

P. Robert et al.

[Title Page](#)

[Abstract](#)

[Introduction](#)

[Conclusions](#)

[References](#)

[Tables](#)

[Figures](#)



[Back](#)

[Close](#)

[Full Screen / Esc](#)

[Printer-friendly Version](#)

[Interactive Discussion](#)

Table 1. Parameters chosen for the routine production at CAA for the continuous calibration of the waveform as a function of the sample frequency.

	Sample freq. (Hz)	NKern	Window duration (s)	Spin period (s)	Nshift
NBR	25	1024	40.95	~ 10	2
HBR	450	4096	9.10	~ 2.3	2



CLUSTER STAFF search coils magnetometer calibration

P. Robert et al.

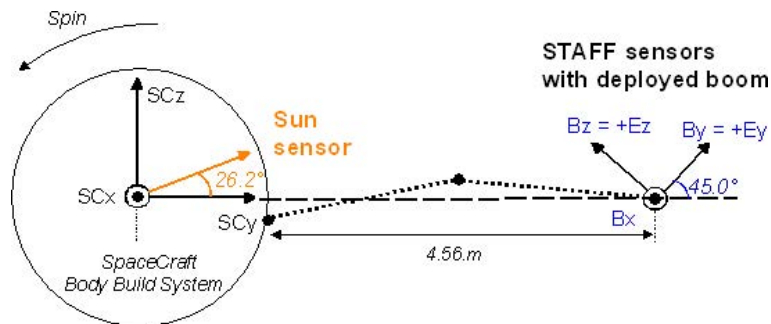


Fig. 1. Position of STAFF search coils antennas on Cluster Spacecraft, with respect to the spacecraft and EFW antennas.

[Title Page](#)

[Abstract](#)

[Introduction](#)

[Conclusions](#)

[References](#)

[Tables](#)

[Figures](#)

[⏪](#)

[⏩](#)

[◀](#)

[▶](#)

[Back](#)

[Close](#)

[Full Screen / Esc](#)

[Printer-friendly Version](#)

[Interactive Discussion](#)

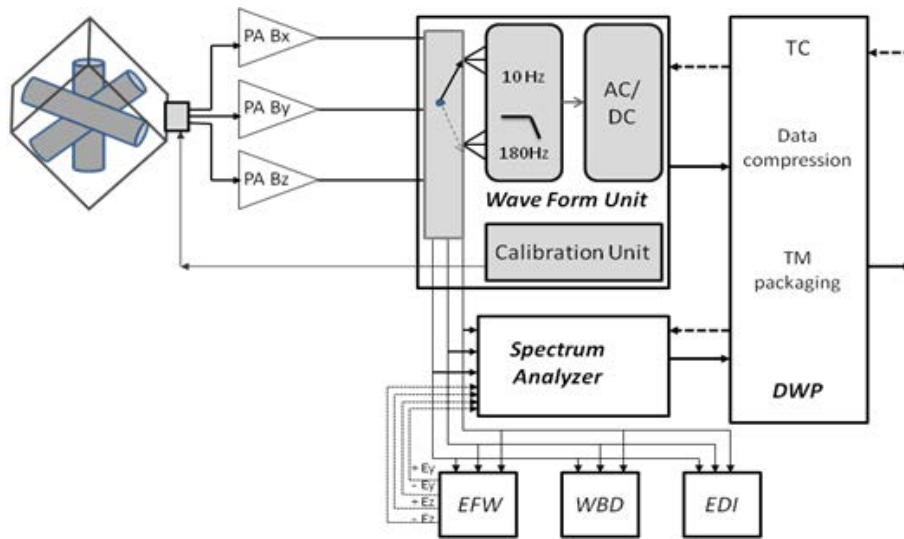


Fig. 2. Block diagram of STAFF experiment and its links to other Cluster experiments.

**CLUSTER STAFF
search coils
magnetometer
calibration**

P. Robert et al.

Title Page	
Abstract	Introduction
Conclusions	References
Tables	Figures
⏪	⏩
◀	▶
Back	Close
Full Screen / Esc	
Printer-friendly Version	
Interactive Discussion	



CLUSTER STAFF
search coils
magnetometer
calibration

P. Robert et al.

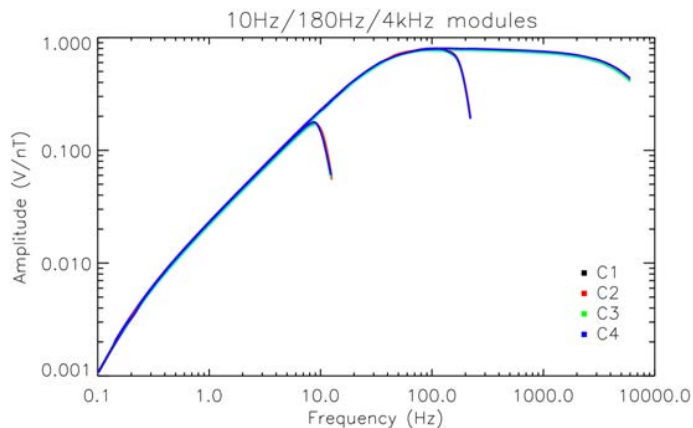


Fig. 3. Amplitude of the transfer functions as a function of the frequency, at the output of the preamplifier for the whole frequency range 0.1 Hz–4 kHz, and at the output of the 180 Hz and the 10 Hz filters respectively, for the B_x component. Data for the four spacecraft are overplotted.

[Title Page](#)[Abstract](#)[Introduction](#)[Conclusions](#)[References](#)[Tables](#)[Figures](#)[⏪](#)[⏩](#)[◀](#)[▶](#)[Back](#)[Close](#)[Full Screen / Esc](#)[Printer-friendly Version](#)[Interactive Discussion](#)

CLUSTER STAFF
search coils
magnetometer
calibration

P. Robert et al.

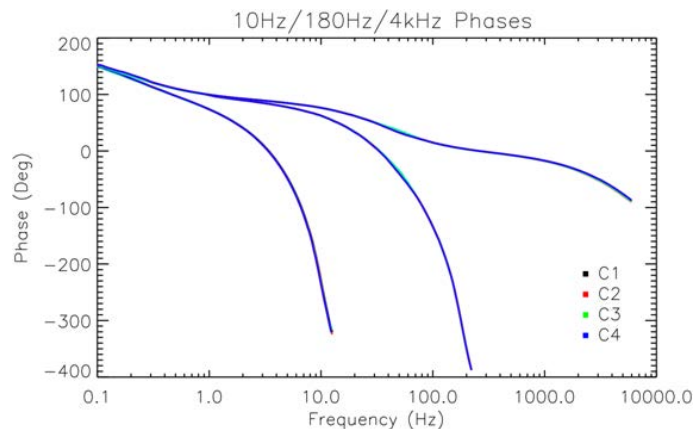


Fig. 4. Phase of the transfer functions in degrees as a function of the frequency, at the output of the preamplifier for the whole frequency range 0.1 Hz–4 kHz, and at the output of the 180 Hz filter and the 10 Hz filter respectively, for the B_x component. Data for the four spacecraft are overplotted.

[Title Page](#)[Abstract](#)[Introduction](#)[Conclusions](#)[References](#)[Tables](#)[Figures](#)[⏪](#)[⏩](#)[◀](#)[▶](#)[Back](#)[Close](#)[Full Screen / Esc](#)[Printer-friendly Version](#)[Interactive Discussion](#)

CLUSTER STAFF
search coils
magnetometer
calibration

P. Robert et al.

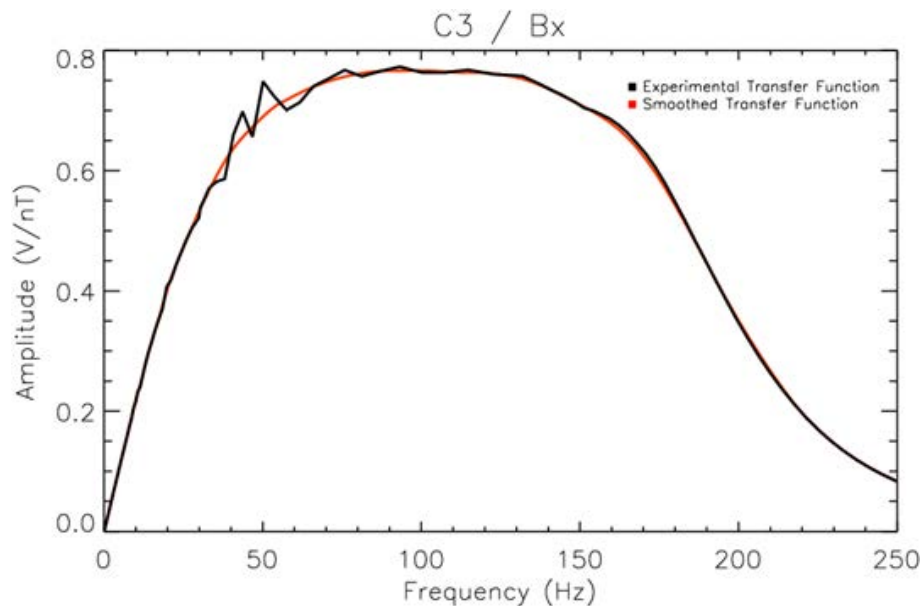
[Title Page](#)[Abstract](#)[Introduction](#)[Conclusions](#)[References](#)[Tables](#)[Figures](#)[⏪](#)[⏩](#)[◀](#)[▶](#)[Back](#)[Close](#)[Full Screen / Esc](#)[Printer-friendly Version](#)[Interactive Discussion](#)

Fig. 5. Example of smoothed transfer function, here B_x component for SC3, at the output of the 180 Hz filter. Influence of power lines at 50 and 150 Hz is clear; this has been smoothed.

CLUSTER STAFF
search coils
magnetometer
calibration

P. Robert et al.

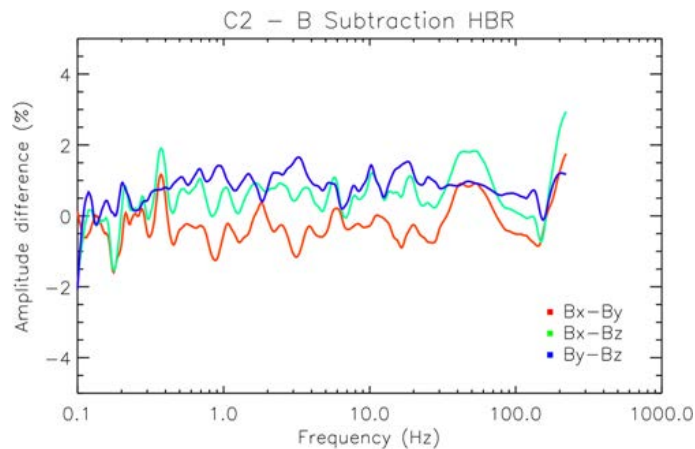


Fig. 6. Example for SC2 of the normalised difference in the answer in amplitude of the 3 components of the magnetic waveform data on spacecraft.

[Title Page](#)[Abstract](#)[Introduction](#)[Conclusions](#)[References](#)[Tables](#)[Figures](#)[⏪](#)[⏩](#)[◀](#)[▶](#)[Back](#)[Close](#)[Full Screen / Esc](#)[Printer-friendly Version](#)[Interactive Discussion](#)

CLUSTER STAFF search coils magnetometer calibration

P. Robert et al.

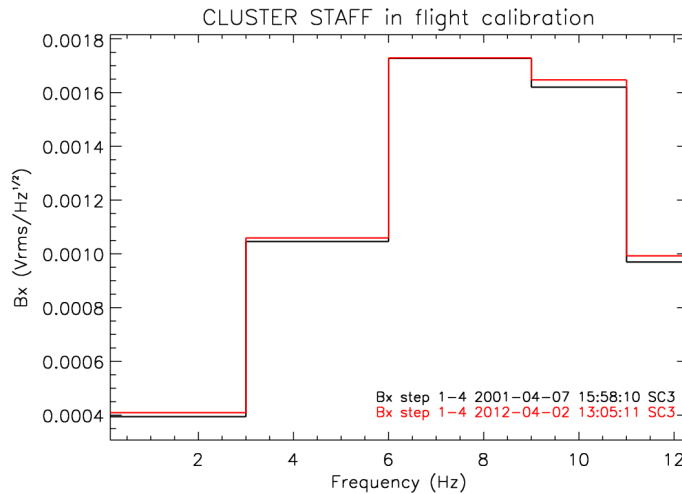


Fig. 7. Superimposition of the result of 2 periods of in flight calibration in 2001 and 2012. Here a pseudo white noise sent to the search coils antennas is measured at the output of the 10 Hz filter.

Title Page	
Abstract	Introduction
Conclusions	References
Tables	Figures
⏪	⏩
◀	▶
Back	Close
Full Screen / Esc	
Printer-friendly Version	
Interactive Discussion	



CLUSTER STAFF search coils magnetometer calibration

P. Robert et al.

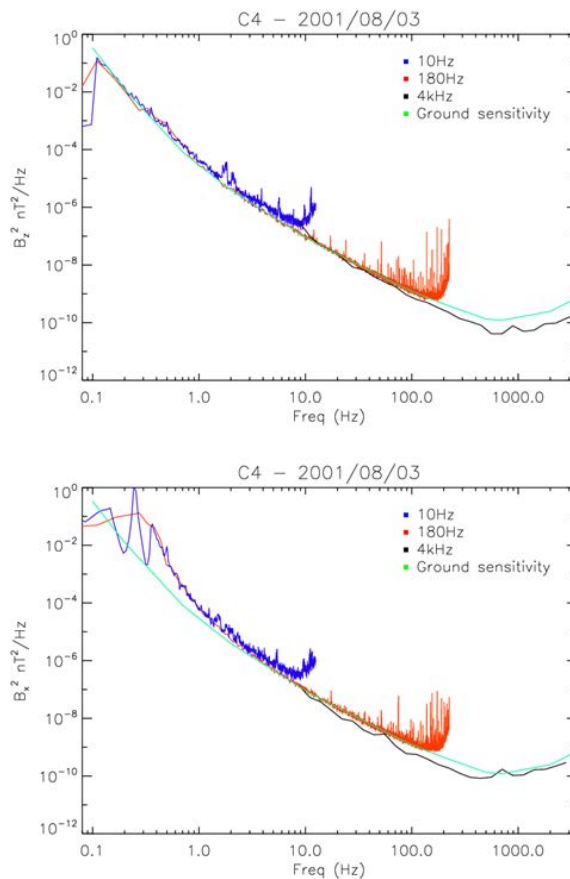


Fig. 8. Example of comparison of the sensitivity measured on ground (green line) in the quiet site of Chambon la Forêt and in flight during a quiet period, for SC4 B_z (top panel) and B_x (bottom panel) components (B_y is identical to B_x). Output of Spectrum Analyser (black line), of 180 Hz filter (red) and 10 Hz filter (blue) are superimposed (see text).

Title Page

Abstract

Introduction

Conclusions

References

Tables

Figures

◀

▶

◀

▶

Back

Close

Full Screen / Esc

Printer-friendly Version

Interactive Discussion

CLUSTER STAFF search coils magnetometer calibration

P. Robert et al.

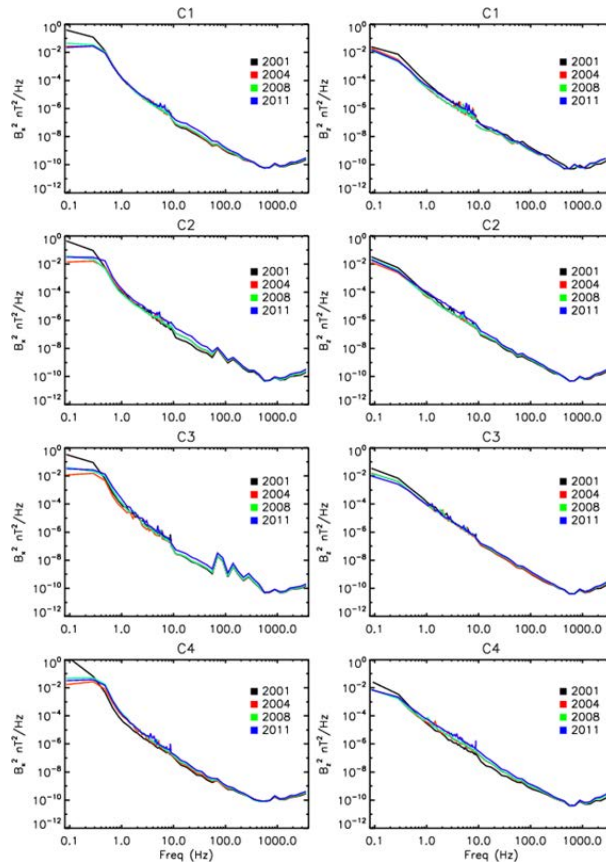


Fig. 9. Evolution of the sensitivity with time, for four different years, in the lobes (quiet region) for the four spacecraft and for the B_x and B_z components (B_y , not shown, is similar to B_x) for both parts of the experiment (waveform up to 9 Hz, Spectrum Analyzer above 9 Hz). The chosen time intervals are 3 August 2001 12:00–13:00 UT, 12 August 2004 11:00–12:00 UT, 12 August 2008 19:00–20:00 UT and 19 August 2011 00:10–01:10.

[Title Page](#)
[Abstract](#)
[Introduction](#)
[Conclusions](#)
[References](#)
[Tables](#)
[Figures](#)
[⏪](#)
[⏩](#)
[◀](#)
[▶](#)
[Back](#)
[Close](#)
[Full Screen / Esc](#)
[Printer-friendly Version](#)
[Interactive Discussion](#)

**CLUSTER STAFF
search coils
magnetometer
calibration**

P. Robert et al.

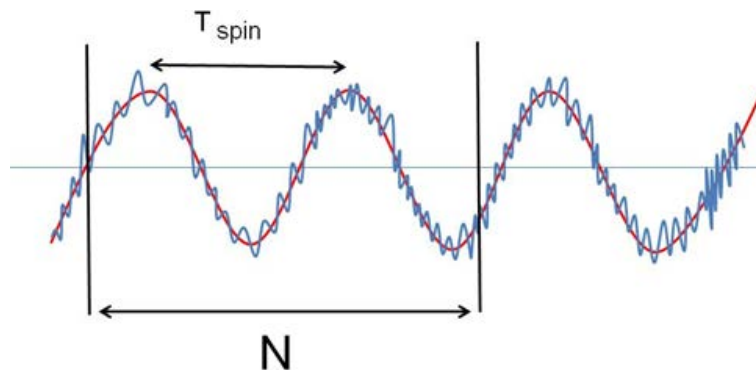
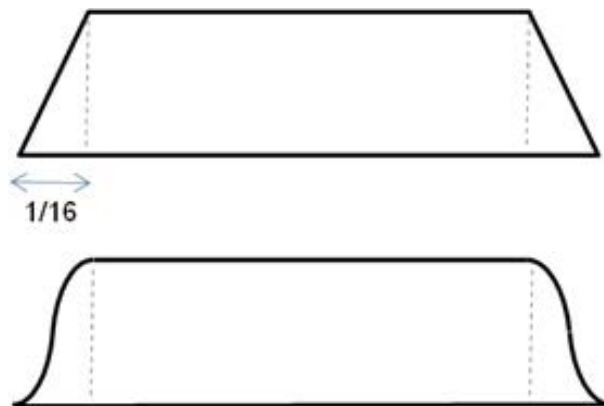


Fig. 10. Spin tone superimposed to rapid variations of the magnetic field that the search coils intend to measure.

[Title Page](#)[Abstract](#)[Introduction](#)[Conclusions](#)[References](#)[Tables](#)[Figures](#)[◀](#)[▶](#)[◀](#)[▶](#)[Back](#)[Close](#)[Full Screen / Esc](#)[Printer-friendly Version](#)[Interactive Discussion](#)

**CLUSTER STAFF
search coils
magnetometer
calibration**

P. Robert et al.

**Fig. 11.** Trapeze and round trapeze used as weighting function.[Title Page](#)[Abstract](#)[Introduction](#)[Conclusions](#)[References](#)[Tables](#)[Figures](#)[⏪](#)[⏩](#)[◀](#)[▶](#)[Back](#)[Close](#)[Full Screen / Esc](#)[Printer-friendly Version](#)[Interactive Discussion](#)

CLUSTER STAFF search coils magnetometer calibration

P. Robert et al.

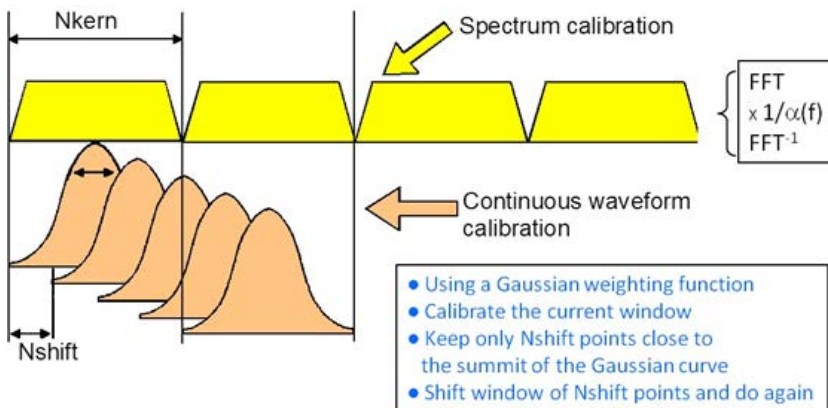


Fig. 12. Illustration of the continuous calibration method (bottom) as compared to spectrum calibration.

[Title Page](#)
[Abstract](#)
[Introduction](#)
[Conclusions](#)
[References](#)
[Tables](#)
[Figures](#)
[⏪](#)
[⏩](#)
[◀](#)
[▶](#)
[Back](#)
[Close](#)
[Full Screen / Esc](#)
[Printer-friendly Version](#)
[Interactive Discussion](#)

**CLUSTER STAFF
search coils
magnetometer
calibration**

P. Robert et al.

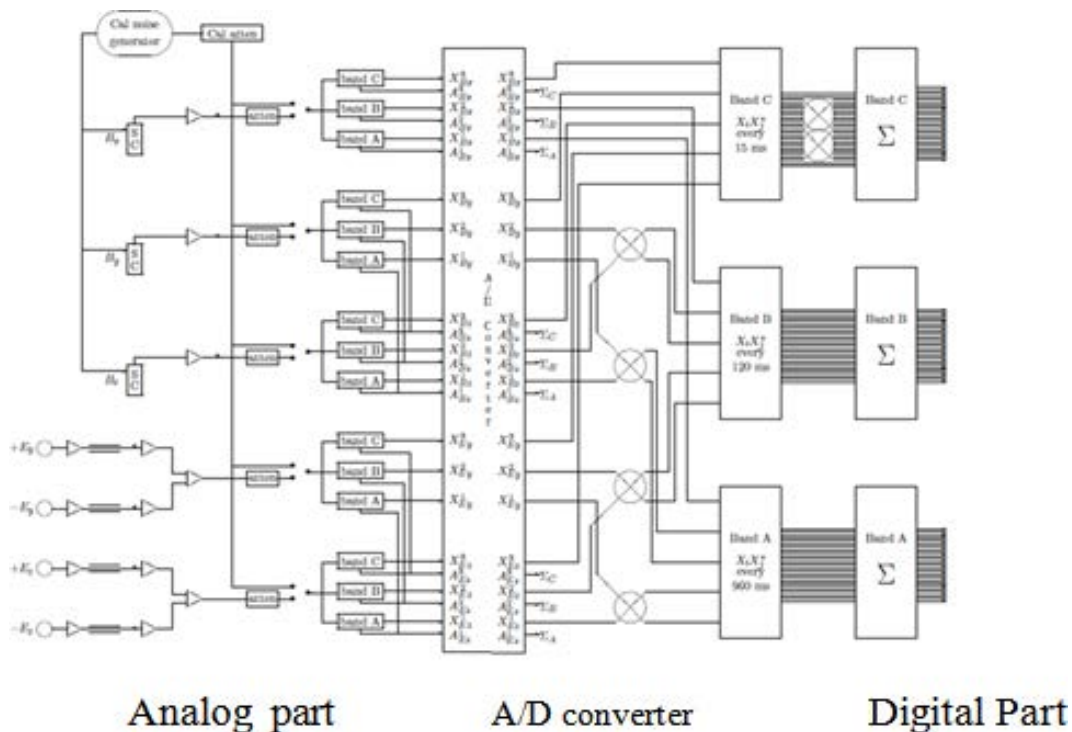


Fig. 13. The different parts of the STAFF Spectrum Analyser Instrument STAFF SA. From left to right: analog part, A/D converter, digital part.

Title Page	
Abstract	Introduction
Conclusions	References
Tables	Figures
◀	▶
◀	▶
Back	Close
Full Screen / Esc	
Printer-friendly Version	
Interactive Discussion	

**CLUSTER STAFF
search coils
magnetometer
calibration**

P. Robert et al.

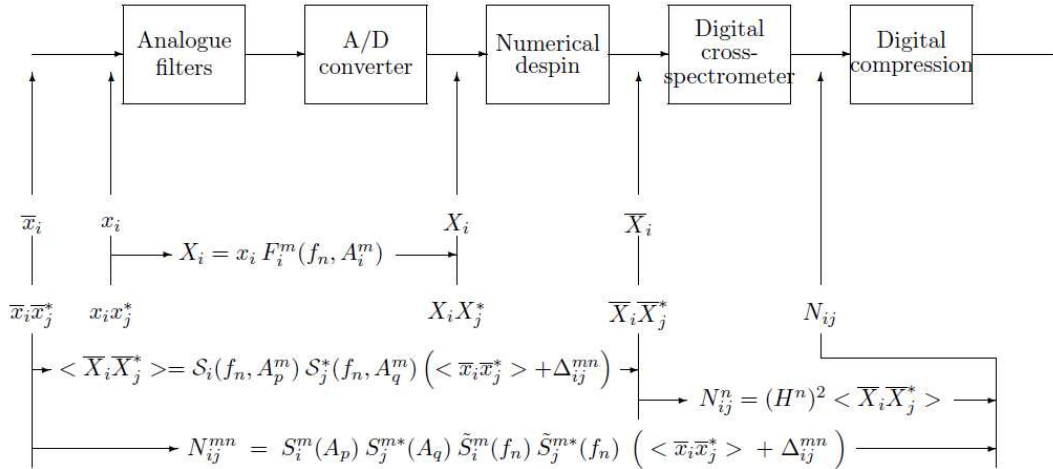


Fig. 14. Relationships between the different signals in STAFF SA.

Title Page	
Abstract	Introduction
Conclusions	References
Tables	Figures
⏪	⏩
◀	▶
Back	Close
Full Screen / Esc	
Printer-friendly Version	
Interactive Discussion	



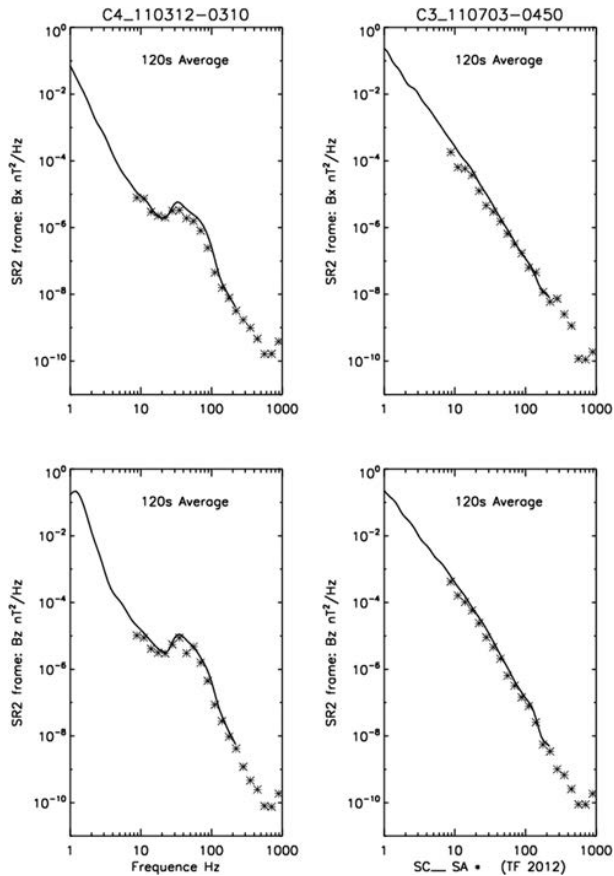


Fig. 15. Examples of a comparison between a wavelet spectrum of the waveform data and a STAFF-SA spectrum. A special operation mode has been used to maximize the overlap between the 2 experiments, between 8 and 180 Hz. Here are the B_z and B_x components for 2 different events (left and right sides respectively).

**CLUSTER STAFF
search coils
magnetometer
calibration**

P. Robert et al.

[Title Page](#)

[Abstract](#)

[Introduction](#)

[Conclusions](#)

[References](#)

[Tables](#)

[Figures](#)

[⏪](#)

[⏩](#)

[◀](#)

[▶](#)

[Back](#)

[Close](#)

[Full Screen / Esc](#)

[Printer-friendly Version](#)

[Interactive Discussion](#)



**CLUSTER STAFF
search coils
magnetometer
calibration**

P. Robert et al.

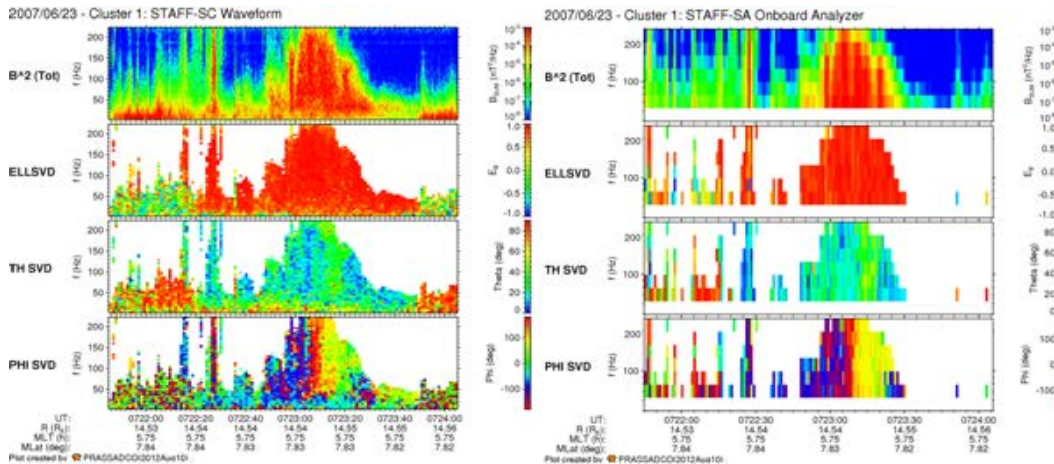


Fig. 16. For each instrument (wave form data – STAFF SC, and Spectrum Analyser STAFF SA), same polarisation and propagation characteristic quantities are plotted in a frequency-time diagram: from top to bottom, the total magnetic PSD (power spectral densities), the ellipticity, the propagation angle $\theta(k, B)$ and the azimuth angle (ϕ). To highlight the polarization of the intense emissions, parameters are plotted only for PSD values, above a threshold. Note that the frequency scale is linear for STAFF-SC and log for STAFF-SA.

[Title Page](#)
[Abstract](#) [Introduction](#)
[Conclusions](#) [References](#)
[Tables](#) [Figures](#)
[◀](#) [▶](#)
[◀](#) [▶](#)
[Back](#) [Close](#)
[Full Screen / Esc](#)
[Printer-friendly Version](#)
[Interactive Discussion](#)



**CLUSTER STAFF
search coils
magnetometer
calibration**

P. Robert et al.

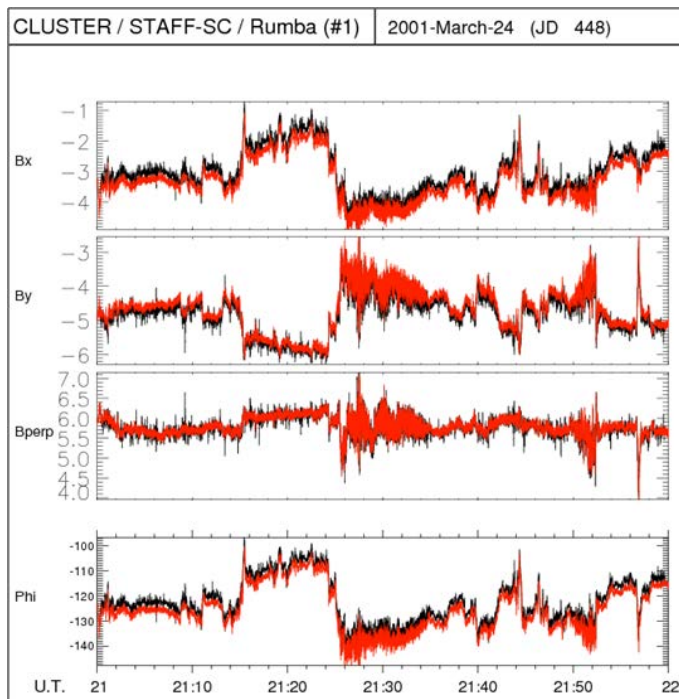


Fig. 17. Direct waveform comparison at large scale (15th Cross-Calibration Workshop/17–19 April 2012).

[Title Page](#)[Abstract](#)[Introduction](#)[Conclusions](#)[References](#)[Tables](#)[Figures](#)[◀](#)[▶](#)[◀](#)[▶](#)[Back](#)[Close](#)[Full Screen / Esc](#)[Printer-friendly Version](#)[Interactive Discussion](#)

**CLUSTER STAFF
search coils
magnetometer
calibration**

P. Robert et al.

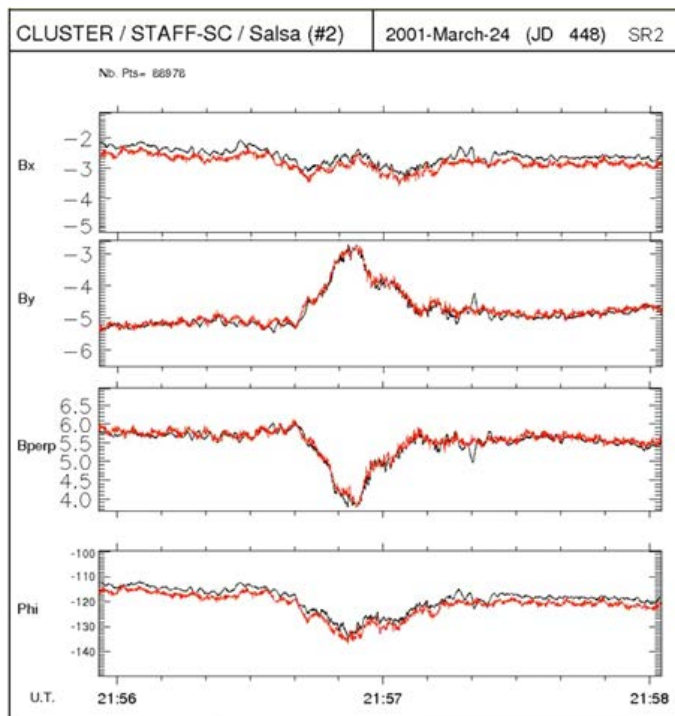


Fig. 18. Zoom on 2 min of data around the spike seen at 21:57 UT of Fig. 17. (15th Cross-Calibration Workshop/17–19 April 2012).

[Title Page](#)[Abstract](#)[Introduction](#)[Conclusions](#)[References](#)[Tables](#)[Figures](#)[◀](#)[▶](#)[◀](#)[▶](#)[Back](#)[Close](#)[Full Screen / Esc](#)[Printer-friendly Version](#)[Interactive Discussion](#)

CLUSTER STAFF search coils magnetometer calibration

P. Robert et al.

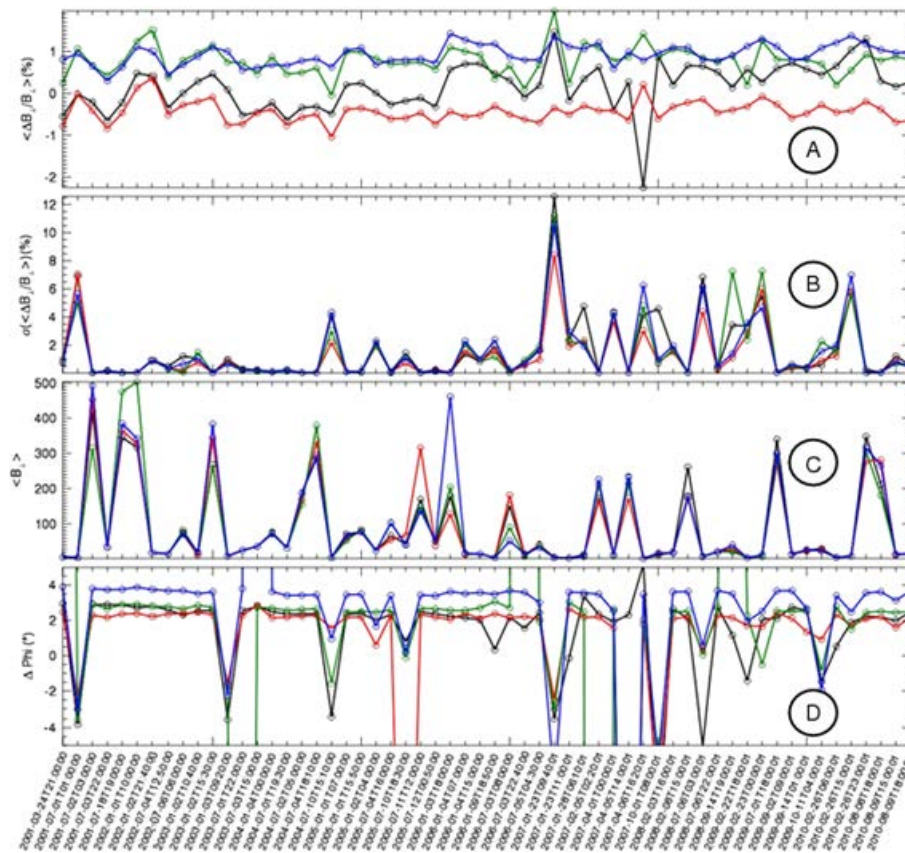


Fig. 19. Statistic over 10 yr of STAFF-FGM spin plane DC field comparison for the four spacecraft (black, red, green, and blue for spacecraft 1, 2, 3, and 4, respectively).

Title Page

Abstract

Introduction

Conclusions

References

Tables

Figures

◀

▶

◀

▶

Back

Close

Full Screen / Esc

Printer-friendly Version

Interactive Discussion

CLUSTER STAFF search coils magnetometer calibration

P. Robert et al.

[Title Page](#)

[Abstract](#)

[Introduction](#)

[Conclusions](#)

[References](#)

[Tables](#)

[Figures](#)

[⏪](#)

[⏩](#)

[◀](#)

[▶](#)

[Back](#)

[Close](#)

[Full Screen / Esc](#)

[Printer-friendly Version](#)

[Interactive Discussion](#)

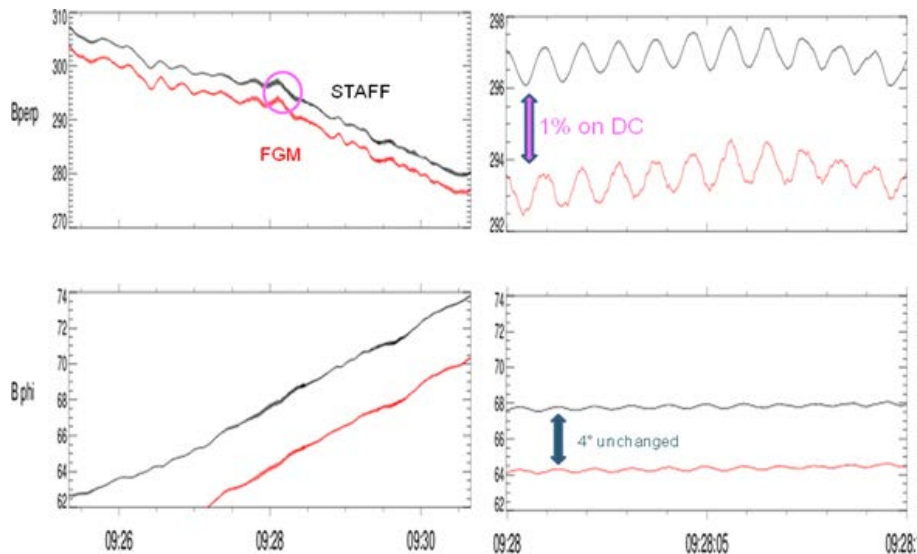


Fig. 20. Wave comparison at 1 Hz (CLUSTER/Tango (#4) 23 September 2001).

**CLUSTER STAFF
search coils
magnetometer
calibration**

P. Robert et al.

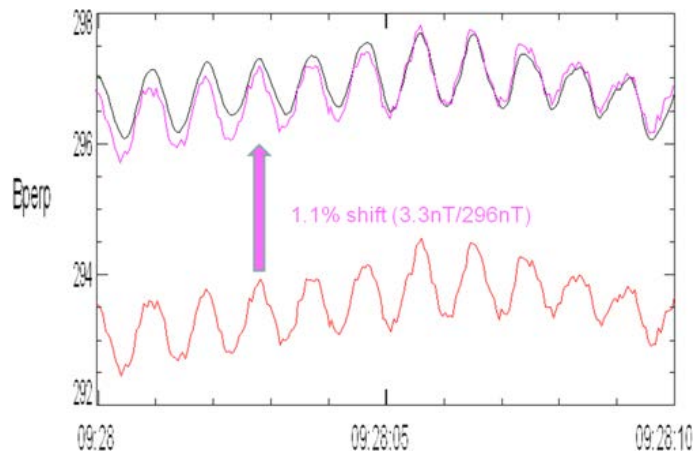


Fig. 21. Wave at 1 Hz, STAFF-FGM superimposed.

[Title Page](#)[Abstract](#)[Introduction](#)[Conclusions](#)[References](#)[Tables](#)[Figures](#)[⏪](#)[⏩](#)[◀](#)[▶](#)[Back](#)[Close](#)[Full Screen / Esc](#)[Printer-friendly Version](#)[Interactive Discussion](#)

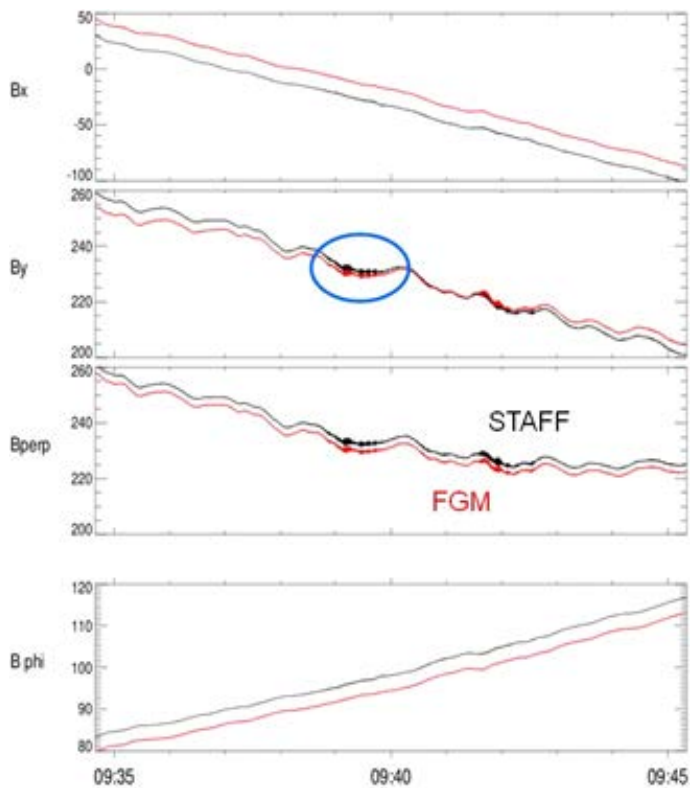


Fig. 22. Wave comparison at 6 Hz (CLUSTER/Tango (#4) 23 September 2001. 14th CAA Cross-Calibration meeting, York, 5–7 October 2011).

**CLUSTER STAFF
search coils
magnetometer
calibration**

P. Robert et al.

[Title Page](#)

[Abstract](#) [Introduction](#)

[Conclusions](#) [References](#)

[Tables](#) [Figures](#)

[⏪](#) [⏩](#)

[◀](#) [▶](#)

[Back](#) [Close](#)

[Full Screen / Esc](#)

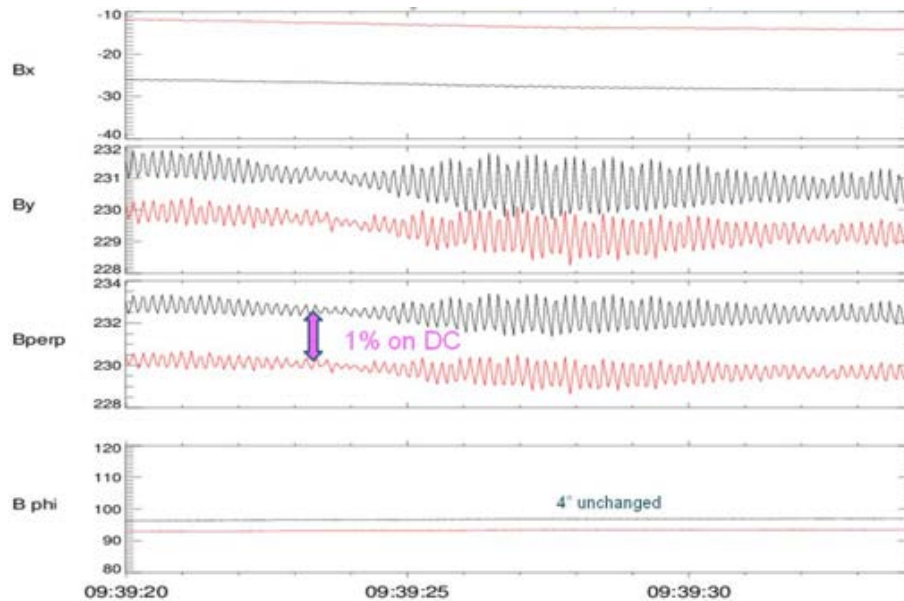
[Printer-friendly Version](#)

[Interactive Discussion](#)



**CLUSTER STAFF
search coils
magnetometer
calibration**

P. Robert et al.

**Fig. 23.** Zoom on wave comparison.[Title Page](#)[Abstract](#)[Introduction](#)[Conclusions](#)[References](#)[Tables](#)[Figures](#)[◀](#)[▶](#)[◀](#)[▶](#)[Back](#)[Close](#)[Full Screen / Esc](#)[Printer-friendly Version](#)[Interactive Discussion](#)

**CLUSTER STAFF
search coils
magnetometer
calibration**

P. Robert et al.

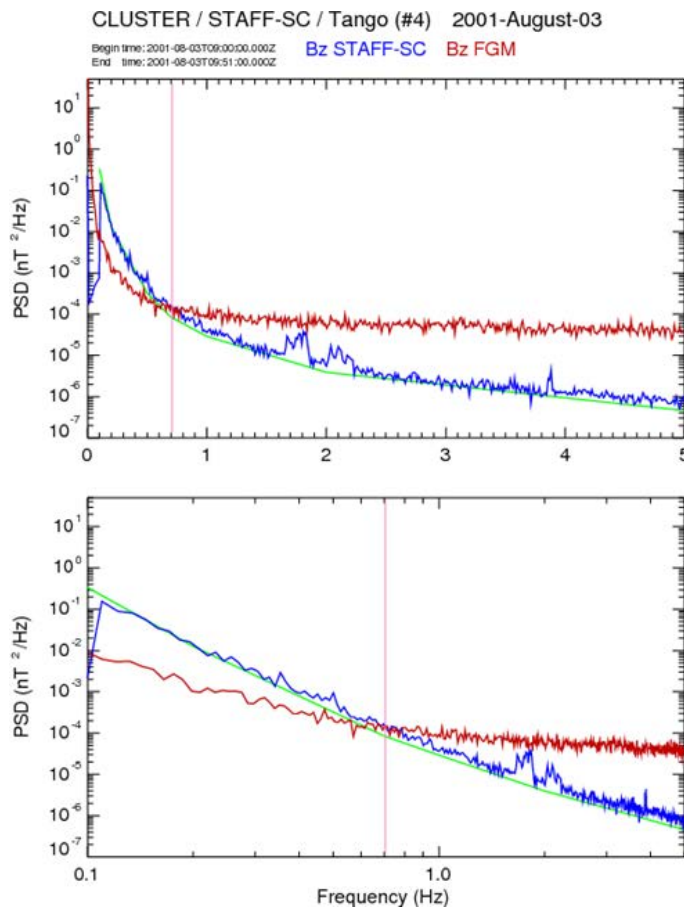


Fig. 24. STAFF-FGM spectra comparison for a very low power event, to show respective sensitivity of the two instruments.

**CLUSTER STAFF
search coils
magnetometer
calibration**

P. Robert et al.

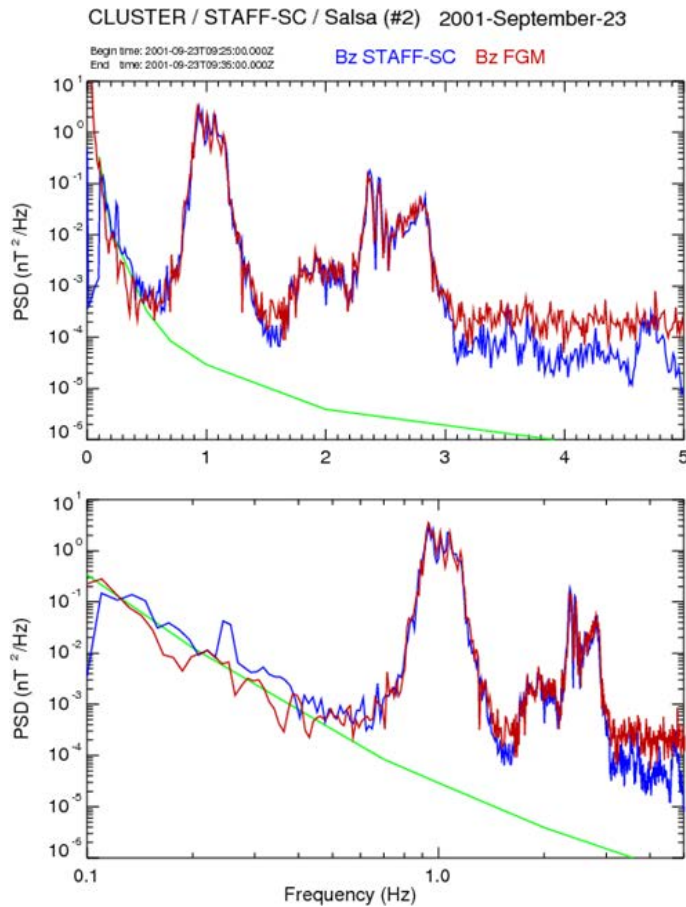


Fig. 25. STAFF-FGM Spectra comparison for event at 1 Hz.

[Title Page](#)

[Abstract](#) [Introduction](#)

[Conclusions](#) [References](#)

[Tables](#) [Figures](#)

[⏪](#) [⏩](#)

[◀](#) [▶](#)

[Back](#) [Close](#)

[Full Screen / Esc](#)

[Printer-friendly Version](#)

[Interactive Discussion](#)



**CLUSTER STAFF
search coils
magnetometer
calibration**

P. Robert et al.

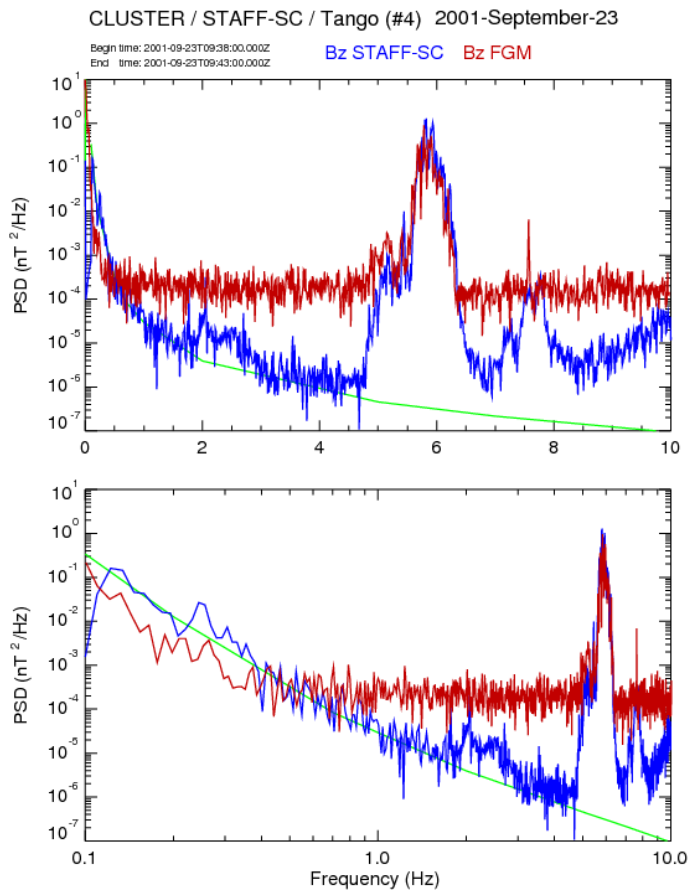


Fig. 26. STAFF-FGM Spectra comparison for event at 6 Hz.

[Title Page](#)

[Abstract](#) [Introduction](#)

[Conclusions](#) [References](#)

[Tables](#) [Figures](#)

[⏪](#) [⏩](#)

[⏴](#) [⏵](#)

[Back](#) [Close](#)

[Full Screen / Esc](#)

[Printer-friendly Version](#)

[Interactive Discussion](#)



CLUSTER STAFF search coils magnetometer calibration

P. Robert et al.

[Title Page](#)

[Abstract](#)

[Introduction](#)

[Conclusions](#)

[References](#)

[Tables](#)

[Figures](#)

[⏪](#)

[⏩](#)

[◀](#)

[▶](#)

[Back](#)

[Close](#)

[Full Screen / Esc](#)

[Printer-friendly Version](#)

[Interactive Discussion](#)

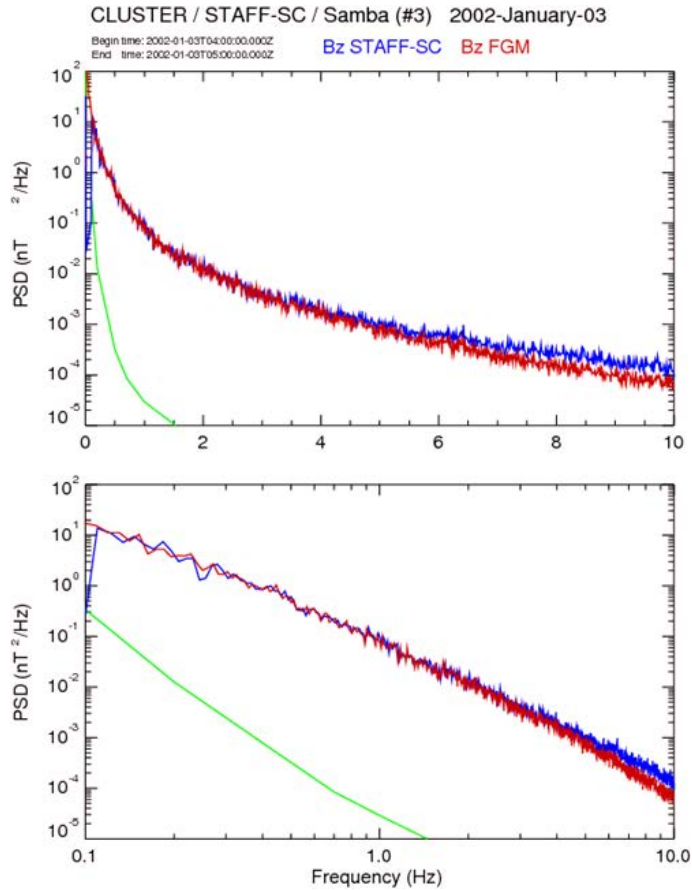


Fig. 27. STAFF-FGM Spectra comparison for a large frequency band event.

CLUSTER STAFF search coils magnetometer calibration

P. Robert et al.

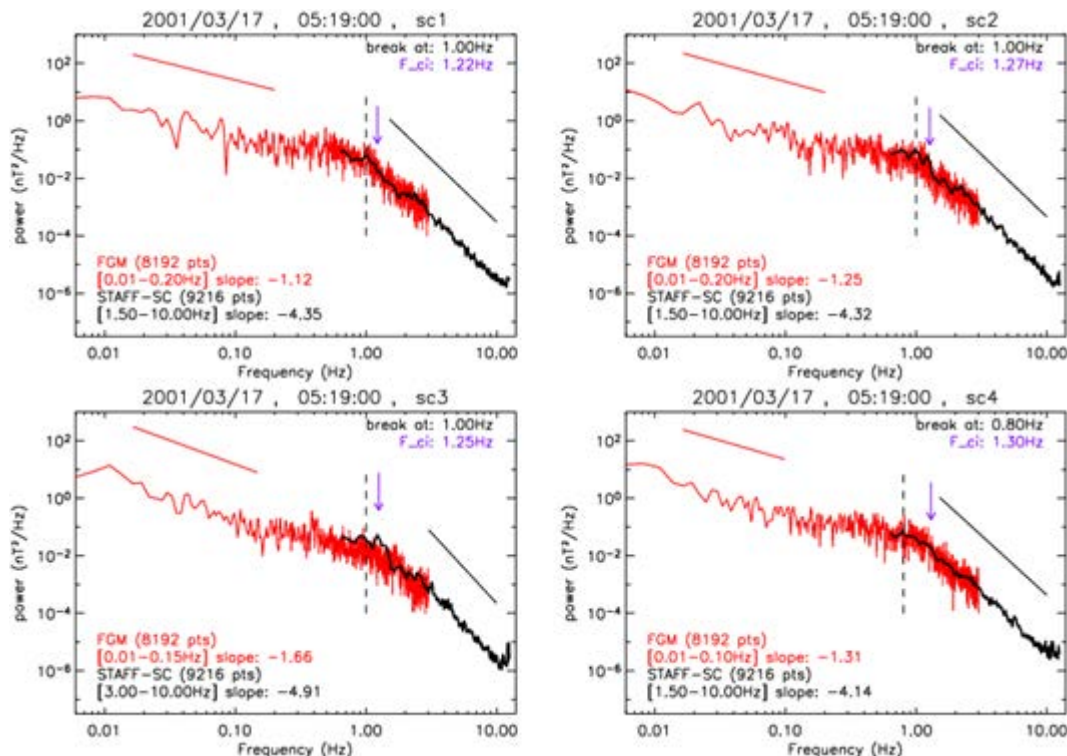


Fig. 28. An example of comparison between FGM (in red) and STAFF (in black) power spectra, from Nikiri et al. (2006), in the cusp region. One can notice the good agreement in the overlap frequency bands, between 0.5 and 2 Hz. It shows that one can use a combination of the 2 complementary experiments, for instance to calculate spectral power law index and frequency break.

[Title Page](#)
[Abstract](#)
[Introduction](#)
[Conclusions](#)
[References](#)
[Tables](#)
[Figures](#)
[⏪](#)
[⏩](#)
[◀](#)
[▶](#)
[Back](#)
[Close](#)
[Full Screen / Esc](#)
[Printer-friendly Version](#)
[Interactive Discussion](#)

S_desc: S_rasc. S_freq: -67.12 74.92 0.249374
 Begin time: 2001-08-03T09:00:00.000Z
 End time: 2001-08-03T09:52:00.000Z
 Number of spectrum: 36 36 36
 Data from Step 4: Data in SR2 system [nT] without DC (Fc=0.1 Fskt=0.1)
 N= 2048 dt= 81.919 s df=0.0122 Hz Fc= 0.10 F1= 0.00 F2= 12.50

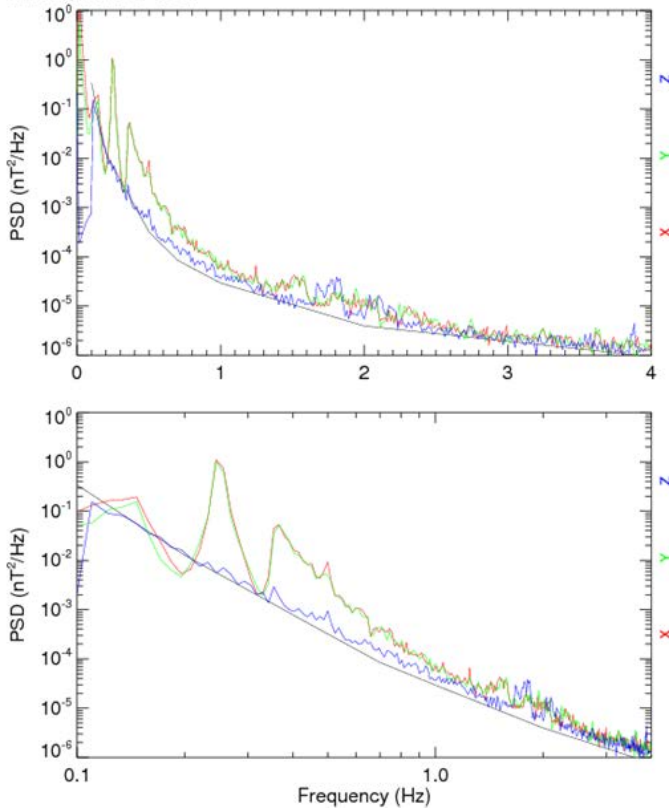


Fig. 29. STAFF Power spectral density of background noise in SR2 system.

**CLUSTER STAFF
 search coils
 magnetometer
 calibration**

P. Robert et al.

[Title Page](#)

[Abstract](#) [Introduction](#)

[Conclusions](#) [References](#)

[Tables](#) [Figures](#)

[⏪](#) [⏩](#)

[⏴](#) [⏵](#)

[Back](#) [Close](#)

[Full Screen / Esc](#)

[Printer-friendly Version](#)

[Interactive Discussion](#)



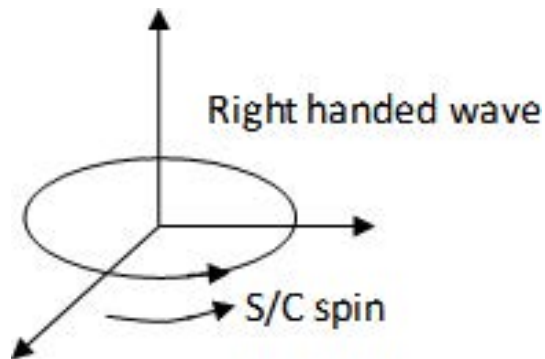


Fig. 30. Schematic diagram illustrating the Doppler Effect on the recorded waves.

CLUSTER STAFF search coils magnetometer calibration

P. Robert et al.

[Title Page](#)

[Abstract](#)

[Introduction](#)

[Conclusions](#)

[References](#)

[Tables](#)

[Figures](#)

[⏪](#)

[⏩](#)

[◀](#)

[▶](#)

[Back](#)

[Close](#)

[Full Screen / Esc](#)

[Printer-friendly Version](#)

[Interactive Discussion](#)



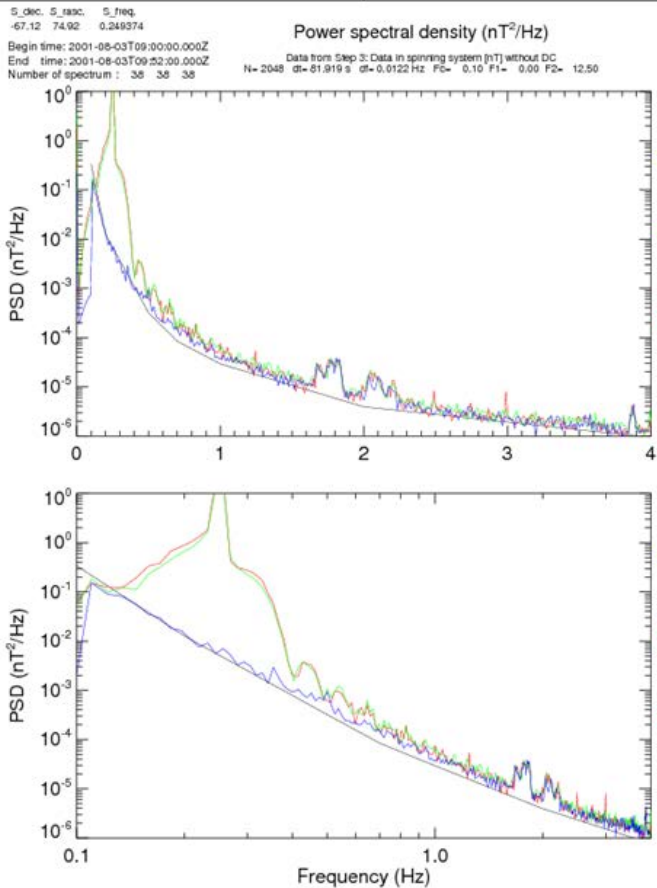


Fig. 31. STAFF Power spectral density of background noise in spinning system.

**CLUSTER STAFF
 search coils
 magnetometer
 calibration**

P. Robert et al.

[Title Page](#)

[Abstract](#) [Introduction](#)

[Conclusions](#) [References](#)

[Tables](#) [Figures](#)

[⏪](#) [⏩](#)

[⏴](#) [⏵](#)

[Back](#) [Close](#)

[Full Screen / Esc](#)

[Printer-friendly Version](#)

[Interactive Discussion](#)

